ANNALS OF PHYSICS: **27**, 79–113 (1964)

Deuteron Photodisintegration and N–P Capture below Pion Production Threshold*†

F. PARTOVI

Laboratory for Nuclear Science and Physics Department, Massachusetts Institute of Technology, Cambridge, Massachusetts

A nonrelativistic, phenomenological treatment of deuteron photodisintegration and n–p capture is presented. The only approximations made are the neglect of nucleon structure, pion exchange currents, and multipoles higher than the octupole. In addition to the total and differential cross section, all parameters necessary to specify the final polarization with an arbitrarily polarized incident beam are calculated. Photodisintegration is calculated at laboratory photon energies of 10, 20, 40, 60, 80, 100, 120, and 140 MeV, and n–p capture at laboratory neutron energies of 0.1 and 0.548 MeV. Hamada's potential is used for computation of the wave functions. Photodisintegration calculations are done in several approximations to exhibit the effect of various terms.

It has been found that spin $E1$ and spin $M2$ transitions to triplet states, usually omitted, are important. The thermal neutron capture cross section found from exact wave functions shows an improvement of 2% over the zero-range approximation, thus accounting for some of the discrepancy with experiment. It is hoped that this improvement will close the 5% gap between experiment and zero-range theory when a potential that fits the singlet scattering length better than Hamada's is used. Results are compared to experiment where possible.

I. INTRODUCTION

Deuteron photodisintegration at energies below pion production threshold have been dealt with by numerous authors. Excellent reference to their works may be found in the most recent papers on the same subject by DeSwart and Marshak (*1*), Breit *et al.* (*2*, *3*), Kramer and Werntz (*4*), and Donnachie (*5*). DeSwart and Marshak included $E1$ and $E2$ transitions as given by Siegert's theorem plus $M1$ spin-flip transitions. They took full account of the coupling in the final states. Breit *et al.* took the above terms into account plus the triplet $M1$ transitions. Kramer and Werntz pointed out the important effect of the

* This work was supported in part through A.E.C. Contract AT(30-1)-2098, by funds provided by the U.S. Atomic Energy Commission.

† Based upon a thesis submitted by the author to the Massachusetts Institute of Technology in partial fulfillment of the requirements for the degree of Doctor of Philosophy.

triplet $M2$ transitions on the differential cross section. They showed that triplet $M2$ transitions through interference with $E1$ transitions raised the isotropic term, a, and lowered the sine squared term, b, in such a way as to leave the total cross section unchanged. Our results confirm their finding, indicating that the transition is mainly due to spin rather than orbital angular momentum and that its effect becomes large enough at 140 MeV to make b negative. Kramer and Werntz, however, neglected the important contribution of the triplet $E1$ transitions induced by spin, considering instead the relatively unimportant contribution of the singlet $E1$ transitions due to spin. They also made a retardation correction to the ordinary $E1$ terms without also including the relativistic correction to $(E_f - E_i)$, a correction which changes the ordinary $E1$ transitions in the opposite direction to the retardation correction. Donnachie includes the relatively insignificant contribution from singlet $M2$ transitions, but neglects the important triplet $M2$ transitions and triplet $E1$ transitions due to spin.

The present work includes:

a. Complete and systematic treatment of the electromagnetic interaction, excluding meson effects. In actual computations, however, multipole terms higher than dipole-octupole interference have been neglected.

b. Exact treatment of the deuteron and continuum wave functions within the phenomenological, nonrelativistic Schroedinger theory.

c. Inclusion of transitions between all possible pairs of states.

d. Calculation of all functions necessary to describe the cross section and the final polarization for arbitrarily polarized incident particles.

e. Comparison of several approximations made in the electromagnetic interaction.

Section II will consist of the theory and the necessary developments. Section III will contain the results and the discussion thereof.

Another paper dealing with the effect of parity violation on the deuteron photodisintegration and n–p capture (hereafter referred to as II) is being prepared (*6*). The requirement that both papers have a common format has dictated the choice of notation used below.

II. THEORY

Units and Coordinates

The atomic system of units will be used throughout. In this system $\hbar = c = 1$, and only one unit, namely, that of length is needed.

Three frames of reference will be defined:

a. The laboratory frame of reference denoted by "lab" in which the deuteron is at rest and the photon has the momentum ω_{lab}.

b. The center-of-mass frame of reference denoted by "CM," in which the

total momentum is zero and the photon has the momentum $\boldsymbol{\omega}$. Position vectors are denoted by $\mathbf{x}$ in this frame.

c. The frame associated with the center-of-mass of the proton-neutron system alone. This frame, denoted by "cm," coincides with lab before disintegration and with CM after disintegration.

ω and ω_{lab} are related by

$$\omega = \omega_{\text{lab}} \left(1 + \frac{2\omega_{\text{lab}}}{M_{\text{d}}}\right)^{-1/2} \tag{1}$$

where M_{d} is the deuteron mass.

In the frame cm two coordinate systems Σ and Σ', differing in their orientation, will be defined. Coordinate system Σ will be oriented with its z-axis parallel to the relative momentum,

$$\mathbf{k} = {}^1\!/_2(\mathbf{k}_1 - \mathbf{k}_2), \tag{2}$$

of the nucleon–nucleon system. (The nucleons will be labeled 1 and 2 throughout the derivation, so that the results may be computed with either nucleon as the proton depending on the corresponding experimental situation.) Coordinate system Σ' will have its z'-axis parallel to the momentum of the photon. For photodisintegration the x'-axis of Σ' will be parallel to the direction of the linear polarization of the photon (if any), and the Euler angles to go from Σ' to Σ will be $(\theta, \phi, 0)$ (Fig. 1). For n–p capture the x-axis of Σ will be parallel to the transverse polarization of nucleon 1 (if any), and the Euler angles to go from Σ to Σ' will be $(\theta, \phi, 0)$ (Fig. 2). Position vectors in the Σ system are denoted by $\xi = (\xi, \vartheta, \varphi) = (x, y, z)$, and in Σ' by $\xi' = (\xi, \vartheta', \varphi') = (x', y', z')$.

The N–P System

The nucleons will be assumed to interact through a semiphenomenological potential developed by Hamada (7). This potential is claimed to provide the

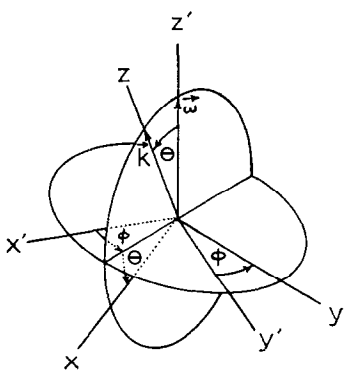

Fig. 1. Relative orientation of Σ and Σ' systems for deuteron photodisintegration

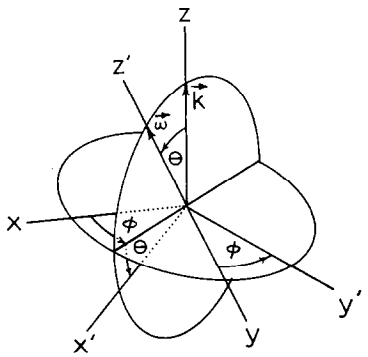

FIG. 2. Relative orientation of Σ and Σ' systems for n–p capture

best fit to the scattering data below 315 MeV. It predicts a 7% d-state probability and phase shifts in fair agreement with the solutions YLAM ($T = 1$) and YLAN3M ($T = 0$) found by the Yale group. It gives a singlet scattering length, however, that is 40% lower than reported from coherent scattering experiments. This potential conserves parity, total spin, total angular momentum and its projection, and isotopic spin. Because of the tensor term in Hamada's potential orbital angular momentum is not conserved. The wave functions of the n–p system referred to the coordinate system Σ, will therefore be expanded in terms of the eigenfunctions $\mathcal{Y}^m_{lsj}$ of $\mathbf{L}^2$, $\mathbf{S}^2$, $\mathbf{J}^2$, J_z defined below.

$$\mathcal{Y}^m_{lsj} \equiv i^l \sum_{m'\ m''} (lm'sm''|jm) Y^{(l)}_{m'}\ \chi^{(s)}_{m''}\,, \tag{3}$$

where $(j_1m_1j_2m_2|jm)$ is the Clebsch-Gordan coefficient, $Y^{(l)}_{m'}$ is the spherical harmonic of rank l and projection m', and $\chi^{(s)}_{m''}$ is the eigenfunction of total spin s and projection m''. This definition differs from the usual definition by a phase factor i^l. The deuteron wave function with projection quantum number m^d is

$$\Psi^d_{m^d} = (N/r)[u_0(r)\mathcal{Y}^{m^d}_{011} + u_2(r)\mathcal{Y}^{m^d}_{211}]. \tag{4}$$

The functions $u_0(r)$ and $u_2(r)$ satisfy the following differential equations

$$\left[\frac{d^2}{dr^2} + k^2 - M(011 \mid V \mid 011)\right] u_0(r) - M(011 \mid V \mid 211)\, u_2(r) = 0, \tag{5}$$

$$\left[\frac{d^2}{dr^2} + k^2 - \frac{6}{r^2} - M(211 \mid V \mid 211)\right] u_2(r) - M(211 \mid V \mid 011)\, u_0(r) = 0, \tag{6}$$

where $\mathbf{r}$ is the relative coordinate of the nucleons,

$$\mathbf{r} = \boldsymbol{\xi}_1 - \boldsymbol{\xi}_2\,, \tag{7}$$

M is the nucleon mass, V is the potential energy operator, and

$$(l's'j' \mid V \mid lsj) \equiv \int (\mathcal{Y}^m_{l's'j'})^* \, V \, \mathcal{Y}^m_{lsj} \, d\tau. \tag{8}$$

The boundary conditions on $u_0(r)$ and $u_2(r)$ are

$$u_0(0) = u_2(0) = 0, \tag{9}$$

$$u_0(r) \xrightarrow{r\to\infty} e^{-\alpha r}, \tag{10}$$

$$u_2(r) \xrightarrow{r\to\infty} N_2 \, e^{-\alpha r}\left(1 + \frac{3}{\alpha r} + \frac{3}{(\alpha r)^2}\right),$$

$$\alpha^2 \equiv ME_b, \tag{11}$$

E_b being the deuteron binding energy as predicted by the potential used. N is so determined that

$$N^2 \int_0^\infty [u_0^2(r) + u_2^2(r)] \, dr = 1. \tag{12}$$

Note that our N_2 is the negative of the customary value because of the i^l in our definition of $\mathcal{Y}^m_{lsj}$, Eq. (3).

The outgoing (incoming) scattering solution with spin s and projection m^s is (with plus sign for the outgoing solution)

$$\Psi^{(\pm)}_{s\,m^s} = \Omega_N^{-1/2}(kr)^{-1}\sum_{\lambda j l l' s'}[4\pi(2l+1)]^{1/2}(los m^s \mid jm^s) \times \exp(\pm i\delta_\lambda{}^j) U^j_{ls\,\lambda} U^j_{l's'\,\lambda} v^j_{l's'\,\lambda}(kr) \mathcal{Y}^{m^s}_{l's'\,j}, \tag{13}$$

where Ω_N is the normalization volume, and k is the magnitude of the relative momentum given by,[1]

$$k^2 = M\left[\omega_{\text{lab}}\left(1 - \frac{E_b}{2M}\right) - E_b\left(1 - \frac{E_b}{4M}\right)\right]. \tag{14}$$

The constants U and the functions v satisfy the differential equation,

$$\left[\frac{d^2}{dr^2} + k^2 - \frac{l(l+1)}{r^2}\right] U^j_{ls\,\lambda} v^j_{ls\,\lambda}(kr) - M\sum_{l'}(lsj \mid V \mid l'sj) U^j_{l's\,\lambda} v^j_{l's\,\lambda}(kr) = 0, \tag{15}$$

and the boundary conditions,

$$v^j_{ls\,\lambda}(0) = 0, \tag{16}$$

$$v^j_{ls\,\lambda}(kr) \xrightarrow{kr\to\infty} \sin(kr - \tfrac{1}{2}l\pi + \delta_\lambda{}^j). \tag{17}$$

[1] Here the value of the binding energy, E_b, will correspond to the experimentally determined value of the binding energy (if different from that given by the potential used).

Equation (15) represents four equations for each j, corresponding to the four possible combinations of l and s (two in the case of $j = 0$). Two of these equations, ($l = j$, $s = 0$) and ($l = j$, $s = 1$), are uncoupled, and the corresponding v's will be labeled by $\lambda = 2$ and 4, respectively. The two other equations ($l = j \pm 1$, $s = 1$) are coupled and have two independent sets of regular solutions. These are labeled by $\lambda = 1$ and 3. We assign $\lambda = 1$ to the solution that goes over to the pure $l = j - 1$ function in the limit of no coupling.[2] The 4×4 matrix U^j whose rows are labeled by (ls) and whose columns by λ has the form

$$U^j = \begin{array}{cc} & \begin{array}{cccc} \lambda = 1 & \lambda = 2 & \lambda = 3 & \lambda = 4 \end{array} \\ \begin{array}{cc} l = j - 1 & s = 1 \\ l = j & s = 0 \\ l = j + 1 & s = 1 \\ l = j & s = 1 \end{array} & \left(\begin{array}{cccc} \cos \epsilon^j & 0 & -\sin \epsilon^j & 0 \\ 0 & 1 & 0 & 0 \\ \sin \epsilon^j & 0 & \cos \epsilon^j & 0 \\ 0 & 0 & 0 & 1 \end{array} \right) \end{array} \tag{18}$$

Here ϵ^j is the coupling coefficient and is the negative of the usually defined coupling coefficient because of the i^l in (3). It goes to zero as the tensor coupling vanishes.

Note that the product of two elements in each column of the U-matrix is zero unless they correspond to the same s. Thus the sum over s' in (13) is purely formal and only $s' = s$ contributes. For the proof of the orthogonality of the U-matrix see the more general case discussed in II.

The Radiation Field

Following the methods used by DeSwart (*8*), we expand the vector potential operator of the radiation field in plane waves of circular polarization.

$$\mathbf{A}(\mathbf{x}) = \Omega_N^{-1/2} \sum_{\boldsymbol{\omega}} \sum_{\mu=\pm 1} (2\pi/\omega)^{1/2} (a_{\boldsymbol{\omega}\mu}\, \boldsymbol{\varepsilon}_\mu\, e^{i\boldsymbol{\omega}\cdot\mathbf{x}} - a^\dagger_{\boldsymbol{\omega}\mu} \boldsymbol{\varepsilon}_{-\mu}\, e^{-i\boldsymbol{\omega}\cdot\mathbf{x}}), \tag{19}$$

where $a_{\boldsymbol{\omega}\mu}$ is the annihilation operator for a photon of momentum $\boldsymbol{\omega}$ and polarization μ, and where all quantities are expressed in the frame CM. The $\boldsymbol{\varepsilon}_\mu$ are spherical unit vectors defined below in terms of Cartesian unit vectors:

$$\boldsymbol{\varepsilon}_{\pm 1} = \mp 2^{-1/2} (\boldsymbol{\varepsilon}_{x'} \pm \boldsymbol{\varepsilon}_{y'}), \tag{20}$$

$$\boldsymbol{\varepsilon}_0 = \boldsymbol{\varepsilon}_{z'}\,. \tag{21}$$

[2] This seemingly strange labeling of states, i.e., grouping states of the same isotopic spin (instead of ordinary spin), is the preferable notation of II, where isotopic spin (but not ordinary spin) is a constant of motion.

Interaction with the Radiation Field

The n–p system interacts with the electromagnetic field through the interaction Hamiltonian

$$H' = -\int \mathbf{J}(\mathbf{x})\cdot\mathbf{A}(\mathbf{x})\, d\mathbf{x}, \tag{22}$$

where $\mathbf{J}(\mathbf{x})$ is the current density operator associated with the n–p system.

The Transition

In an identical method to that of DeSwart (*8*), we will describe the initial and final states of the transition by density matrices ζ_{in} and ζ_{f} connected by means of a transition matrix.

Description of the Initial and the Final States

For the photodisintegration process the initial density matrix (for unaligned target deuterons) is

$$\zeta_{\text{in}} = \tfrac{1}{6}(1 - \boldsymbol{\Sigma}\cdot\boldsymbol{\sigma}), \tag{23}$$

where the $\boldsymbol{\sigma}$ are the three Pauli spin matrices labeled by the two states of circular polarization, $\mu = \pm 1$, and $\boldsymbol{\Sigma}(\Sigma_{x'}, \Sigma_{y'}, \Sigma_{z'})$ are the Stoke's parameters for the polarization of the radiation (*9*). The degree of linear polarization, Σ_l, is given by

$$\Sigma_l = (\Sigma_{x'}^2 + \Sigma_{y'}^2)^{1/2}. \tag{24}$$

The angle ψ between the x'-axis and the direction of linear polarization is given by

$$\Sigma_{x'} = \Sigma_l \cos 2\psi, \tag{25}$$

$$\Sigma_{y'} = \Sigma_l \sin 2\psi. \tag{26}$$

ψ is zero owing to our choice of the x'-axis in the Σ' coordinate system to be along the photon polarization. The extent of circular polarization Σ_c is

$$\Sigma_c = \Sigma_{z'}. \tag{27}$$

Σ_c may be positive or negative depending on the direction of the net circular polarization.

The Transition Matrix

The transition matrix for photodisintegration is

$$(s\, m^s \mid T \mid \mu\, m^d) = \Omega_{\text{N}} \left(\frac{kM}{8\pi^2}\right)^{1/2} H'_{\text{fi}}, \tag{28}$$

where $H'_{\rm fi}$ is the matrix element of H' between the final state characterized by an "incoming" state of total spin s and projection m^s of the neutron–proton system and the initial state characterized by the photon polarization μ and the deuteron projection quantum number m^d. The final density matrix is given by

$$\zeta_{\rm f} = T\zeta_{\rm in}T^{\dagger}, \tag{29}$$

from which we can find the differential cross section $d\sigma/d\Omega$ and polarization $\mathbf{P}(\alpha)$ of outgoing nucleon α:

$$d\sigma/d\Omega = {\rm tr}\zeta_{\rm f}\,, \tag{30}$$

$$\mathbf{P}(\alpha) = {\rm tr}[\zeta_{\rm f}\boldsymbol{\sigma}(\alpha)]/{\rm tr}\zeta_{\rm f}\,, \qquad \alpha = 1 \text{ or } 2, \tag{31}$$

where $\boldsymbol{\sigma}(\alpha)$ is twice the spin operator for nucleon α in the $(s\ m^s)$ representation.

For the capture process (quantities referring to which are distinguished by a superscript c), the initial density matrix, with nucleon 2 assumed to be unpolarized, is given by

$$\zeta^{\rm c}_{\rm in} = \tfrac{1}{4}[1 + \mathbf{P}(1)\cdot\boldsymbol{\sigma}(1)]. \tag{32}$$

The transition matrix $T^{\rm c}$ for the capture process is given by

$$(\mu\ m^d \mid T^{\rm c} \mid s\ m^s) = \Omega_{\rm N}\left(\frac{M\omega^2}{8\pi^2 k}\right)^{1/2}(H'_{\rm fi})^{\rm c}, \tag{33}$$

where $(H'_{\rm fi})^{\rm c}$ is the matrix element of H' between the final state characterized by the photon polarization μ and deuteron projection quantum number m^d and the initial state characterized by an "outgoing" n–p state of total spin s and projection m^s. The final density matrix is given by

$$\zeta_{\rm f}{}^{\rm c} = T^{\rm c}\zeta^{\rm c}_{\rm in}(T^{\rm c})^{\dagger}, \tag{34}$$

from which we can find the differential cross section $d\sigma^{\rm c}/d\Omega$ and photon polarization parameters $\Sigma_{x'}$, $\Sigma_{y'}$, $\Sigma_{z'}$:

$$d\sigma^{\rm c}/d\Omega = {\rm tr}\zeta_{\rm f}{}^{\rm c} \tag{35}$$

$$\Sigma_k = -{\rm tr}(\sigma_k\zeta_{\rm f}{}^{\rm c})/{\rm tr}\zeta_{\rm f}{}^{\rm c}; \qquad k = x',\ y',\ z'. \tag{36}$$

CALCULATION OF $H'_{\rm fi}$

Since the current density operator associated with the uniform motion of the n–p center-of-mass does not contribute to the transition, one need only consider the current arising from the internal motion of the n–p system, in which case $H'_{\rm fi}$ can be written,

$$H'_{\rm fi} = -\Omega_{\rm N}^{-1/2}(2\pi/\omega)^{1/2}\left(\Psi^{(-)}_{s\ m^s}\left|\int \mathbf{J}^{\rm int}(\boldsymbol{\xi})\cdot\boldsymbol{\varepsilon}_\mu\, e^{i\boldsymbol{\omega}\cdot\boldsymbol{\xi}}\,d\boldsymbol{\xi}\right|\Psi^d_{m^d}\right). \tag{37}$$

For further calculation it is convenient to expand $\boldsymbol{\varepsilon}_\mu \exp(i\boldsymbol{\omega}\cdot\boldsymbol{\xi})$ in electric and magnetic multipoles,

$$\begin{aligned}\boldsymbol{\varepsilon}_\mu e^{i\boldsymbol{\omega}\cdot\boldsymbol{\xi}} = \sum_{LM} D^{(L)}_{M\mu}(0,-\theta,-\phi)\\ \times\Bigg\{-\left(\frac{2\pi(2L+1)}{L(L+1)}\right)^{1/2} i^{L+1}\frac{1}{\omega}\boldsymbol{\nabla}_\xi\left[\left(1+\xi\frac{d}{d\xi}\right)j_L(\omega\xi)Y^{(L)}_M(\vartheta,\varphi)\right]\\ -\left(\frac{2\pi(2L+1)}{L(L+1)}\right)^{1/2} i^{L+1}\,\omega\boldsymbol{\xi}\,j_L(\omega\xi)\;Y^{(L)}_M(\vartheta,\varphi)\\ -\mu\left(\frac{2\pi(2L+1)}{L(L+1)}\right)^{1/2} i^L j_L(\omega\xi)\,[\mathbf{L}Y^{(L)}_M(\vartheta,\varphi)]\Bigg\}.\end{aligned} \tag{38}$$

The rotation function $D^{(L)}_{M\mu}(0,-\theta,-\phi)$ appearing above is defined by (*10*)

$$\begin{aligned}D^{(j)}_{mm'}(\alpha,\beta,\gamma) &\equiv (j\,m|e^{-i\alpha J_z}e^{-i\beta J_y}e^{-i\gamma J_z}|j\,m')\\ &= e^{-im\alpha}d^{(j)}_{mm'}(\beta)e^{-im'\gamma},\end{aligned} \tag{39}$$

$$d^{(j)}_{mm'}(\beta) \equiv (j\,m|e^{-i\beta J_y}|j\,m'). \tag{40}$$

The first two terms in the summand of Eq. (38) constitute the electric 2^L-pole, the last term the magnetic 2^L-pole. The first term gives rise to the usual electric multipole transitions resulting from Siegert's theorem. The second term gives rise to spin electric multipole transitions and to a retardation correction to the electric multipole transitions, as we shall see.

The internal current density operator satisfies the differential charge conservation law

$$\boldsymbol{\nabla}_\xi\cdot\mathbf{J}^{\mathrm{int}}(\boldsymbol{\xi}) + i[H_{\mathrm{n-p}}, \zeta(\boldsymbol{\xi})] = 0, \tag{41}$$

where $H_{\mathrm{n-p}}$ is the Hamiltonian operator and $\zeta(\boldsymbol{\xi})$ the charge density operator for the neutron–proton system. $\mathbf{J}^{\mathrm{int}}(\boldsymbol{\xi})$ is composed of "orbital" or "convection" current and spin current:

$$\mathbf{J}^{\mathrm{int}}(\boldsymbol{\xi}) = \mathbf{J}^{\mathrm{c}}(\boldsymbol{\xi}) + \mathbf{J}^{\mathrm{s}}(\boldsymbol{\xi}). \tag{42}$$

Assuming current density and charge density operators are sums of single-particle terms, we have

$$\zeta(\boldsymbol{\xi}) = \sum_{\alpha=1}^{2}\zeta_\alpha(\boldsymbol{\xi}), \tag{43}$$

$$\mathbf{J}^{\mathrm{c}}(\boldsymbol{\xi}) = \frac{1}{2M}\sum_{\alpha=1}^{2}[\zeta_\alpha(\boldsymbol{\xi})\boldsymbol{\pi}_\alpha + \boldsymbol{\pi}_\alpha\zeta_\alpha(\boldsymbol{\xi})], \tag{44}$$

$$\mathbf{J}^{\mathrm{s}}(\boldsymbol{\xi}) = \frac{e}{2M}\sum_{\alpha=1}^{2}[\boldsymbol{\nabla}_\xi\times\mathbf{M}_\alpha(\boldsymbol{\xi})], \tag{45}$$

where $\boldsymbol{\pi}_\alpha$ is the momentum operator and $\mathbf{M}_\alpha(\xi)$ the magnetization operator for nucleon α. Making the further approximation that the nuclear charge and magnetic moment are concentrated at one point, we have,

$$\zeta_\alpha(\xi) = e_\alpha \delta(\xi - \xi_\alpha), \tag{46}$$

$$\mathbf{M}_\alpha(\xi) = \mu_\alpha \boldsymbol{\sigma}(\alpha)\delta(\xi - \xi_\alpha), \tag{47}$$

where e_α and μ_α are the charge and the magnetic moment of nucleon α. Approximations (43)–(45) are equivalent to the neglect of pion exchange contributions, which have been discussed and shown to be small in the literature (*11–13*). These contributions are difficult to calculate theoretically. Their magnitude can be obtained experimentally by calculating the known effects and noting the discrepancy with experiment. Equations (46) and (47) ignore the electromagnetic structure of the nucleons now known experimentally (*14–18*). This can be remedied by an extension of the present calculation with appropriate form factors replacing Eqs. (46) and (47). In connection with the above remarks we note that according to Siegert's theorem pion current effects will only affect terms proportional to ω/M, which are small compared to the electric multipole transitions at low energies. Relying, on the other hand, on the momentum-dependent terms in the potential to account for meson effects, we have found the correction coming from Hamada's spin-orbit term to be totally insignificant.

Using (38) and (42)–(47) in (37), performing the integration with the help of (41), and substituting in (28), we get

$$(s\, m^s | T | \mu\, m^d) = e^{i\mu\phi}(s\, m^s | t | \mu\, m^d), \tag{48}$$

$$(s\, m^s \mid t \mid \mu\, m^d) = \sum_{L=1}^{\infty} d_\mu^{(L)}{}_{m^s - m^d}(\theta)[(s\, m^s \mid \mathcal{E}^{(L)} \mid m^d) + \mu(s\, m^s \mid \mathfrak{M}^{(L)} \mid m^d)], \tag{49}$$

$$(s\, m^s \mid \mathcal{E}^{(L)} \mid m^d) = \sum_{\lambda j l} \left[\frac{4\pi(2L+1)}{2j+1}\right]^{1/2} \exp(i\delta_\lambda{}^j) U^j_{ls\,\lambda} \times (1\, m^d\, L\, m^s - m^d \mid j\, m^s)(l0sm^s \mid jm^s)\mathfrak{I}^{(L)}(\lambda j), \tag{50}$$

$$(s\, m^s \mid \mathfrak{M}^{(L)} \mid m^d) = \sum_{\lambda j l} \left[\frac{4\pi(2L+1)}{2j+1}\right]^{1/2} \exp(i\delta_\lambda{}^j) U^j_{ls\,\lambda} \times (1\, m^d\, L\, m^s - m^d \mid j\, m^s)(l0sm^s \mid jm^s)\mathfrak{S}^{(L)}(\lambda j), \tag{51}$$

$$\mathfrak{I}^{(L)}(\lambda j) = \frac{N}{k}\left(\frac{Mk}{2\omega}\right)^{1/2}\left(\frac{2L+1}{L(L+1)}\right)^{1/2}\left\{-\left(1+\frac{\omega}{2M_d}\right)[e_1 + (-)^L e_2]\right. \times \sum_{l's'\,l''s''} U^j_{l's'\,\lambda}\left[I_1(l's'\lambda j; L; l'') + \frac{L}{2L+1} I_2(l's'\,\lambda j; L-1; l'') - \frac{L+1}{2L+1} I_2(l's'\lambda j; L+1; l'')\right] \tag{52}$$

$$
\begin{aligned}
&\times (l's'j \,\|\, Y^{(L)} \,\|\, l''s''1)i^L \\
&+\frac{\omega}{4M}\,[e_1+(-)^L e_2]\sum_{l's'\,l''s''} U^j_{l's'\,\lambda}\Big[2I_3(l's'\lambda j;L;l'')+I_1(l's'\lambda j;L;l'') \\
&\quad+\frac{L}{2L+1}I_2(l's'\lambda j;L-1;l'')-\frac{L+1}{2L+1}I_2(l's'\lambda j;L+1;l'')\Big] \\
&\quad\times (l's'j\|Y^{(L)}\|l''s''1)i^L \\
&+\frac{e\omega}{2M}\,[L(L+1)]^{1/2}[\mu_1+(-)^L\mu_2]\sum_{l's'\,l''s''} U^j_{l's'\,\lambda} I_1(l's'\lambda j;L;l'') \qquad (52)\\
&\quad\times (l's'j \,\|\, [Y^{(L)}\otimes \mathbf{S}]^{(L)} \,\|\, l''\,s''\,1)i^L \\
&+\frac{e\omega}{2M}\,[L(L+1)]^{1/2}[\mu_1-(-)^L\mu_2]\sum_{l's'\,l''s''} U^j_{l's'\,\lambda} I_1(l's'\lambda j;L;l'') \\
&\quad\times (l's'j \,\|\, [Y^{(L)}\otimes \mathbf{t}]^{(L)} \,\|\, l''\,s''\,1)\,i^L\Big\},
\end{aligned}
$$

$$
\begin{aligned}
S^{(L)}(\lambda j) = \frac{N}{k}\left(\frac{Mk}{2\omega}\right)^{1/2}&\left[\frac{2L+1}{L(L+1)}\right]^{1/2}\Big\{-\frac{\omega}{2M}\left[\frac{L}{2L+1}\right]^{1/2}[e_1-(-)^L e_2] \\
&\times\sum_{l's'\,l''s''} U^j_{l's'\,\lambda} I_1(l's'\lambda j;L-1;l'') \\
&\times (l's'j \,\|\, [Y^{(L-1)}\otimes \mathbf{L}]^{(L)} \,\|\, l''\,s''\,1)\,i^{L-1} \\
&+\frac{\omega}{2M}\left[\frac{L+1}{2L+1}\right]^{1/2}[e_1-(-)^L e_2]\sum_{l's'\,l''s''} U^j_{l's'\,\lambda} I_1(l's'\lambda j;L+1;l'') \\
&\times (l'\,s'\,j \,\|\, [Y^{(L+1)}\otimes \mathbf{L}]^{(L)} \,\|\, l''\,s''\,1)\,i^{L+1} \\
&-\frac{e\omega}{2M}\left[\frac{L(L+1)^2}{2L+1}\right]^{1/2}[\mu_1-(-)^L\mu_2]\sum_{l's'\,l''s''} U^j_{l's'\,\lambda} I_1(l's'\lambda j;L-1;l'') \\
&\times (l'\,s'\,j \,\|\, [Y^{(L-1)}\otimes \mathbf{S}]^{(L)} \,\|\, l''\,s''\,1)\,i^{L-1} \qquad (53)\\
&-\frac{e\omega}{2M}\left[\frac{L(L+1)^2}{2L+1}\right]^{1/2}[\mu_1+(-)^L\mu_2]\sum_{l's'\,l''s''} U^j_{l's'\,\lambda} I_1(l'\,s'\,\lambda j;L-1;l'') \\
&\times (l'\,s'\,j \,\|\, [Y^{(L-1)}\otimes \mathbf{t}]^{(L)} \,\|\, l''\,s''\,1)\,i^{L-1} \\
&-\frac{e\omega}{2M}\left[\frac{L^2(L+1)}{2L+1}\right]^{1/2}[\mu_1-(-)^L\mu_2]\sum_{l's'\,l''s''} U^j_{l's'\,\lambda} I_1(l'\,s'\,\lambda j;L+1;l'') \\
&\times (l'\,s'\,j \,\|\, [Y^{(L+1)}\otimes \mathbf{S}]^{(L)} \,\|\, l''\,s''\,1)\,i^{L+1} \\
&-\frac{e\omega}{2M}\left[\frac{L^2(L+1)}{2L+1}\right]^{1/2}[\mu_1+(-)^L\mu_2]\sum_{l's'\,l''s''} U^j_{l's'\,\lambda} I_1(l's'\lambda j;L+1;l'') \\
&\times (l'\,s'\,j \,\|\, [Y^{(L+1)}\otimes \mathbf{t}]^{(L)} \,\|\, l''\,s''\,1)\,i^{L+1}\Big\},
\end{aligned}
$$

where

$$I_1(l' s' \lambda j; L'; l'') \equiv \int_0^\infty dr\, v^j_{l's'\lambda}(kr) j_{L'}(\omega r/2)\, u_{l''}(r), \tag{54}$$

$$I_2(l' s' \lambda j; L'; l'') \equiv \int_0^\infty dr\, v^j_{l's'\lambda}(kr)\, (\omega r/2)\, j_{L'}(\omega r/2)\, u_{l''}(r), \tag{55}$$

$$I_3(l' s' \lambda j; L'; l'') \equiv \int_0^\infty dr\, v^j_{l's'\lambda}(kr)\, j_{L'}(\omega r/2)\, r \frac{d}{dr} u_{l''}(r), \tag{56}$$

$$\mathbf{S} \equiv \tfrac{1}{2}(\boldsymbol{\sigma}(1) + \boldsymbol{\sigma}(2)), \tag{57}$$

$$\mathbf{t} \equiv \tfrac{1}{2}(\boldsymbol{\sigma}(1) - \boldsymbol{\sigma}(2)). \tag{58}$$

The symbol

$$(\alpha' j' \| Q^{(L)} \| \alpha'' j'')$$

denotes the reduced matrix element of the irreducible tensor operator $Q^{(L)}_M$ as defined by Racah (*19*),

$$(\alpha' j' m' | Q^{(L)}_M | \alpha'' j'' m'') = \frac{(j'' m'' LM | j' m')}{(2j'+1)^{1/2}} (\alpha' j' \| Q^{(L)} \| \alpha'' j''). \tag{59}$$

We have used the symbol,

$$[A^{(L_1)} \otimes B^{(L_2)}]^{(L)}_M,$$

to denote the tensor product of the irreducible tensor operators $A^{(L_1)}_{M_1}$ and $B^{(L_2)}_{M_2}$:

$$[A^{(L_1)} \otimes B^{(L_2)}]^{(L)}_M \equiv \sum_{M_1 M_2} (L_1 M_1 L_2 M_2 | LM) A^{(L_1)}_{M_1} B^{(L_2)}_{M_2}. \tag{60}$$

A vector operator $\mathbf{V}$ is regarded as an irreducible tensor operator of rank 1, expressible in terms of its spherical components

$$\mathbf{V} = \sum_m (-)^m V_m \boldsymbol{\varepsilon}_{-m}. \tag{61}$$

Expressions for the reduced matrix elements appearing in (52) and (53) are given below for the case s', $s'' = 0, 1$.

$$(l's'j' \| Y^{(L)} \| l''s''j'')\, i^L = (-)^{(l'+L-l''+2s''+2j'')/2} \begin{pmatrix} l' & L & l'' \\ 0 & 0 & 0 \end{pmatrix} \begin{Bmatrix} l' & j' & s'' \\ j'' & l'' & L \end{Bmatrix} \times [(2l'+1)(2j'+1)(2L+1)(2l''+1)(2j''+1)/4\pi]^{1/2} \delta_{s's''}, \tag{62}$$

$$(l's'j' \| [Y^{(L')} \otimes \mathbf{S}]^{(L)} \| l''s''j'')\, i^{L'} = (-)^{(l'+L'+l'')/2} \begin{pmatrix} l' & L' & l'' \\ 0 & 0 & 0 \end{pmatrix} \begin{Bmatrix} l' & 1 & j' \\ l'' & 1 & j'' \\ L' & 1 & L \end{Bmatrix} \times [6(2l'+1)(2j'+1)(2L+1)(2L'+1)(2l''+1)(2j''+1)/4\pi]^{1/2} \delta_{s's''} \delta_{s'1}, \tag{63}$$

$$(l's'j' \| [Y^{(L')} \otimes \mathbf{t}]^{(L)} \| l''s''j'')i^{L'}$$

$$= (-)^{(l'+L'+l'')/2}[(-)^{s''}-(-)^{s'}] \begin{pmatrix} l' & L' & l'' \\ 0 & 0 & 0 \end{pmatrix} \begin{Bmatrix} s'' & s' & 1 \\ \frac{1}{2} & \frac{1}{2} & \frac{1}{2} \end{Bmatrix} \begin{Bmatrix} l' & s' & j' \\ l'' & s'' & j'' \\ L' & 1 & L \end{Bmatrix} \quad (64)$$

$$\times [3(2l'+1)(2s'+1)(2j'+1)(2L+1)(2L'+1)$$

$$\cdot(2l''+1)(2s''+1)(2j''+1)/8\pi]^{1/2},$$

$$(l's'j' \| [Y^{(L')} \otimes \mathbf{L}]^{(L)} \| l''s''j'')i^{L'}$$

$$= (-)^{(l'+L'-l''+2s''+2j'')/2} \begin{pmatrix} l' & L' & l'' \\ 0 & 0 & 0 \end{pmatrix} \begin{Bmatrix} s'' & j'' & l'' \\ L & l' & j' \end{Bmatrix} \begin{Bmatrix} L' & 1 & L \\ l'' & l' & l'' \end{Bmatrix} \quad (65)$$

$$\times [l''(l''+1)(2l''+1)^2(2j''+1)(2L+1)$$

$$\times (2L'+1)(2l'+1)(2j'+1)/4\pi]^{1/2} \delta_{s's''}.$$

The 3-j, 6-j and 9-j symbols used above are defined by Rotenberg *et al.* (*20*). We note finally that the sum over deuteron spin s'' is purely formal, for it can only take on the value $s'' = 1$. The matrix elements (50) and (51) have the following symmetry properties resulting from parity conservation.

$$(s\ -m^s \mid \mathcal{E}^{(L)} \mid -m^d) = (-)^{s+1}(s\ m^s \mid \mathcal{E}^{(L)} \mid m^d),$$

$$(s\ -m^s \mid \mathfrak{M}^{(L)} \mid -m^d) = (-)^{s}(s\ m^s \mid \mathfrak{M}^{(L)} \mid m^d).$$

A similar treatment for the capture process yields

$$(\mu\ m^d \mid T^c \mid s\ m^s) = e^{i(m^s-m^d)\phi}(\mu\ m^d \mid t^c \mid s\ m^s), \quad (66)$$

with

$$(\mu\ m^d \mid t^c \mid s\ m^s) = (-)^{m^s-m^d+1}(\omega/k)(s\ m^s \mid t \mid \mu\ m^d). \quad (67)$$

Having expressions for the transition matrix, it is now a simple matter to take the traces indicated by Eq. (30) and Eq. (31) or Eq. (35) and Eq. (36). We get for photodisintegration

$$\frac{d\sigma}{d\Omega} = I_0(\theta)[1 + \Sigma_l\, \Sigma(\theta) \cos 2\phi], \quad (68)$$

$$\frac{d\sigma}{d\Omega} P_x(1) = \Sigma_l\, Q_{x2}(\theta) \sin 2\phi + \Sigma_c\, Q_{x3}(\theta), \quad (69)$$

$$\frac{d\sigma}{d\Omega} P_y(1) = I_0(\theta) P_{y0}(\theta) + \Sigma_l\, Q_{y1}(\theta) \cos 2\phi, \quad (70)$$

$$\frac{d\sigma}{d\Omega} P_z(1) = \Sigma_l\, Q_{z2}(\theta) \sin 2\phi + \Sigma_c\, Q_{z3}(\theta), \quad (71)$$

where θ and ϕ, it should be recalled, are the angles describing the direction of nucleon 1. (See the section beginning with Eq. (23) on the meaning of the symbols, $\mathbf{P}(1) = (P_x(1), P_y(1), P_z(1))$, Σ_l, and Σ_c.) The functions of θ appearing in Eq. (68)–(71) are given by the following.

$$
\begin{aligned}
I_0(\theta) = \frac{1}{6}\sum_{M=0}^{2}\sum_{L'=L}^{\infty}\sum_{L=1}^{\infty}(2-\delta_{M0})(2-\delta_{LL'})\Big\{&[d_{1\ M}^{(L)}(\theta)\, d_{1\ M}^{(L')}(\theta) \\
&+ d_{1\ -M}^{(L)}(\theta)\, d_{1\ -M}^{(L')}(\theta)]\,\mathrm{Re}\sum_{s=0}^{1}\sum_{m^d=-1}^{1}[(sM+m^d\,|\,\mathcal{E}^{(L)}\,|\,m^d) \\
&\cdot(sM+m^d\,|\,\mathcal{E}^{(L')}\,|\,m^d)^* + (sM+m^d\,|\,\mathfrak{M}^{(L)}\,|\,m^d)(sM+m^d\,|\,\mathfrak{M}^{(L')}\,|\,m^d)^*] \\
&+ [d_{1\ M}^{(L)}(\theta)\, d_{1\ M}^{(L')}(\theta) - d_{1\ -M}^{(L)}(\theta)\, d_{1\ -M}^{(L')}(\theta)]\,\mathrm{Re}\sum_{s=0}^{1}\sum_{m^d=-1}^{1}[(sM+m^d\,|\,\mathcal{E}^{(L)}\,|\,m^d) \\
&\cdot(sM+m^d\,|\,\mathfrak{M}^{(L')}\,|\,m^d)^* + (sM+m^d\,|\,\mathfrak{M}^{(L)}\,|\,m^d)(sM+m^d\,|\,\mathcal{E}^{(L')}\,|\,m^d)^*]\Big\},
\end{aligned}
\tag{72}
$$

$$
\begin{aligned}
I_0(\theta)\Sigma(\theta) = \frac{1}{6}\sum_{M=0}^{2}\sum_{L'=L}^{\infty}\sum_{L=1}^{\infty}(-)^M(2-\delta_{M0})(2-\delta_{LL'})\Big\{&[d_{1\ M}^{(L)}(\theta)\, d_{1\ -M}^{(L')}(\theta) \\
&+ d_{1\ -M}^{(L)}(\theta)\, d_{1\ -M}^{(L')}(\theta)]\,\mathrm{Re}\sum_{s=0}^{1}\sum_{m^d=-1}^{1}[(sM+m^d\,|\,\mathcal{E}^{(L)}\,|\,m^d) \\
&\cdot(sM+m^d\,|\,\mathcal{E}^{(L')}\,|\,m^d)^* - (sM+m^d\,|\,\mathfrak{M}^{(L)}\,|\,m^d)(sM+m^d\,|\,\mathfrak{M}^{(L')}\,|\,m^d)^*] \\
&+ [d_{1\ M}^{(L)}(\theta)\, d_{1\ -M}^{(L')}(\theta) - d_{1\ -M}^{(L)}(\theta)\, d_{1\ M}^{(L')}(\theta)]\,\mathrm{Re}\sum_{s=0}^{1}\sum_{m^d=-1}^{1}[-(sM+m^d\,|\,\mathcal{E}^{(L)}\,|\,m^d) \\
&\cdot(sM+m^d\,|\,\mathfrak{M}^{(L')}\,|\,m^d)^* + (sM+m^d\,|\,\mathfrak{M}^{(L)}\,|\,m^d)(sM+m^d\,|\,\mathcal{E}^{(L')}\,|\,m^d)^*]\Big\},
\end{aligned}
\tag{73}
$$

$$
\begin{aligned}
Q_{x2}(\theta) = \frac{\sqrt{2}}{3}\,\mathrm{Im}\sum_{L\,L'\,m^d}(-)^{m^d}\{&[d_{1\ -m^d}^{(L)}(\theta)\, d_{1\ m^d-1}^{(L')}(\theta) \\
&+ d_{1\ m^d}^{(L)}(\theta)\, d_{1\ 1-m^d}^{(L')}(\theta)][(10|\,\mathcal{E}^{(L)}\,|m^d)(11|\,\mathcal{E}^{(L')}\,|m^d)^* \\
&- (10|\,\mathfrak{M}^{(L)}\,|m^d)(11|\,\mathfrak{M}^{(L')}\,|m^d)^* - (00|\,\mathcal{E}^{(L)}\,|m^d)(11|\,\mathcal{E}^{(L')}\,|m^d)^* \\
&+ (00|\,\mathfrak{M}^{(L)}\,|m^d)(11|\,\mathfrak{M}^{(L')}\,|m^d)^*] + [d_{1\ -m^d}^{(L)}(\theta)\, d_{1\ m^d-1}^{(L')}(\theta) \\
&- d_{1\ m^d}^{(L)}(\theta)\, d_{1\ 1-m^d}^{(L')}(\theta)][-(10|\,\mathcal{E}^{(L)}\,|m^d)(11|\,\mathfrak{M}^{(L')}\,|m^d)^* \\
&+ (10|\,\mathfrak{M}^{(L)}\,|m^d)(11|\,\mathcal{E}^{(L')}\,|m^d)^* + (00|\,\mathcal{E}^{(L)}\,|m^d)(11|\,\mathfrak{M}^{(L')}\,|m^d)^* \\
&- (00|\,\mathfrak{M}^{(L)}\,|m^d)(11|\,\mathcal{E}^{(L')}\,|m^d)^*]\},
\end{aligned}
\tag{74}
$$

$$
\begin{aligned}
Q_{x3}(\theta) = & -\frac{\sqrt{2}}{3}\,\mathrm{Re}\sum_{L\,L'\,m^d}\{[d_{1\,-m^d}^{(L)}(\theta)\,d_{1\,1-m^d}^{(L')}(\theta) \\
& + d_{1\,m^d}^{(L)}(\theta)\,d_{1\,m^d-1}^{(L')}(\theta)][(10|\,\mathcal{E}^{(L)}\,|m^d)(11|\,\mathcal{E}^{(L')}\,|m^d)^* \\
& + (10|\,\mathfrak{M}^{(L)}\,|m^d)(11|\,\mathfrak{M}^{(L')}\,|m^d)^* - (00|\,\mathcal{E}^{(L)}\,|m^d)(11|\,\mathcal{E}^{(L')}\,|m^d)^* \\
& - (00|\,\mathfrak{M}^{(L)}\,|m^d)(11|\,\mathfrak{M}^{(L')}\,|m^d)^*] + [d_{1\,-m^d}^{(L)}(\theta)\,d_{1\,1-m^d}^{(L')}(\theta) \\
& - d_{1\,m^d}^{(L)}(\theta)\,d_{1\,m^d-1}^{(L')}(\theta)][(10|\,\mathcal{E}^{(L)}\,|m^d)(11|\,\mathfrak{M}^{(L')}\,|m^d)^* \\
& + (10|\,\mathfrak{M}^{(L)}\,|m^d)(11|\,\mathcal{E}^{(L')}\,|m^d)^* - (00|\,\mathcal{E}^{(L)}\,|m^d)(11|\,\mathfrak{M}^{(L')}\,|m^d)^* \\
& - (00|\,\mathfrak{M}^{(L)}\,|m^d)(11|\,\mathcal{E}^{(L')}\,|m^d)^*]\},
\end{aligned}
\tag{75}
$$

$$
\begin{aligned}
I_0(\theta)\,P_{y0}(\theta) = & \frac{\sqrt{2}}{3}\,\mathrm{Im}\sum_{L\,L'\,m^d}\{[d_{1\,-m^d}^{(L)}(\theta)\,d_{1\,1-m^d}^{(L')}(\theta) \\
& - d_{1\,m^d}^{(L)}(\theta)\,d_{1\,m^d-1}^{(L')}(\theta)][(10|\,\mathcal{E}^{(L)}\,|m^d)(11|\,\mathcal{E}^{(L')}\,|m^d)^* \\
& + (10|\,\mathfrak{M}^{(L)}\,|m^d)(11|\,\mathfrak{M}^{(L')}\,|m^d)^* - (00|\,\mathcal{E}^{(L)}\,|m^d)(11|\,\mathcal{E}^{(L')}\,|m^d)^* \\
& - (00|\,\mathfrak{M}^{(L)}\,|m^d)(11|\,\mathfrak{M}^{(L')}\,|m^d)^*] + [d_{1\,-m^d}^{(L)}(\theta)\,d_{1\,1-m^d}^{(L')}(\theta) \\
& + d_{1\,m^d}^{(L)}(\theta)\,d_{1\,m^d-1}^{(L')}(\theta)][(10|\,\mathcal{E}^{(L)}\,|m^d)(11|\,\mathfrak{M}^{(L')}\,|m^d)^* \\
& + (10|\,\mathfrak{M}^{(L)}\,|m^d)(11|\,\mathcal{E}^{(L')}\,|m^d)^* - (00|\,\mathcal{E}^{(L)}\,|m^d)(11|\,\mathfrak{M}^{(L')}\,|m^d)^* \\
& - (00|\,\mathfrak{M}^{(L)}\,|m^d)(11|\,\mathcal{E}^{(L')}\,|m^d)^*]\},
\end{aligned}
\tag{76}
$$

$$
\begin{aligned}
Q_{y1}(\theta) = & -\frac{\sqrt{2}}{3}\,\mathrm{Im}\sum_{L\,L'\,m^d}(-)^{m^d}\{[d_{1\,-m^d}^{(L)}(\theta)\,d_{1\,m^d-1}^{(L')}(\theta) \\
& - d_{1\,m^d}^{(L)}(\theta)\,d_{1\,1-m^d}^{(L')}(\theta)][(10|\,\mathcal{E}^{(L)}\,|m^d)(11|\,\mathcal{E}^{(L')}\,|m^d)^* \\
& - (10|\,\mathfrak{M}^{(L)}\,|m^d)(11|\,\mathfrak{M}^{(L')}\,|m^d)^* - (00|\,\mathcal{E}^{(L)}\,|m^d)(11|\,\mathcal{E}^{(L')}\,|m^d)^* \\
& + (00|\,\mathfrak{M}^{(L)}\,|m^d)(11|\,\mathfrak{M}^{(L')}\,|m^d)^*] + [d_{1\,-m^d}^{(L)}(\theta)\,d_{1\,m^d-1}^{(L')}(\theta) \\
& + d_{1\,m^d}^{(L)}(\theta)\,d_{1\,1-m^d}^{(L')}(\theta)][-(10|\,\mathcal{E}^{(L)}\,|m^d)(11|\,\mathfrak{M}^{(L')}\,|m^d)^* \\
& + (10|\,\mathfrak{M}^{(L)}\,|m^d)(11|\,\mathcal{E}^{(L')}\,|m^d)^* + (00|\,\mathcal{E}^{(L)}\,|m^d)(11|\,\mathfrak{M}^{(L')}\,|m^d)^* \\
& - (00|\,\mathfrak{M}^{(L)}\,|m^d)(11|\,\mathcal{E}^{(L')}\,|m^d)^*]\},
\end{aligned}
\tag{77}
$$

$$
\begin{aligned}
Q_{z2}(\theta) = & \tfrac{1}{3}\mathrm{Im}\sum_{L\,L'\,m^d}(-)^{m^d}\{[d_{1\,1-m^d}^{(L)}(\theta)\,d_{1\,m^d-1}^{(L')}(\theta) - d_{1\,m^d-1}^{(L)}(\theta)\,d_{1\,1-m^d}^{(L')}(\theta)] \\
& \times [(11|\,\mathcal{E}^{(L)}\,|m^d)(11|\,\mathcal{E}^{(L')}\,|m^d)^* - (11|\,\mathfrak{M}^{(L)}\,|m^d)(11|\,\mathfrak{M}^{(L')}\,|m^d)^*] \\
& + [d_{1\,1-m^d}^{(L)}(\theta)\,d_{1\,m^d-1}^{(L')}(\theta) + d_{1\,m^d-1}^{(L)}(\theta)\,d_{1\,1-m^d}^{(L')}(\theta)] \\
& \times [-(11|\,\mathcal{E}^{(L)}\,|m^d)(11|\,\mathfrak{M}^{(L')}\,|m^d)^* + (11|\,\mathfrak{M}^{(L)}\,|m^d)(11|\,\mathcal{E}^{(L')}\,|m^d)^*] \\
& - 2[(d_{1\,-m^d}^{(L)}(\theta)\,d_{1\,m^d}^{(L')}(\theta)] \\
& \times [(00|\,\mathcal{E}^{(L)}\,|m^d)(10|\,\mathcal{E}^{(L')}\,|m^d)^* - (00|\,\mathfrak{M}^{(L)}\,|m^d)(10|\,\mathfrak{M}^{(L')}\,|m^d)^* \\
& - (00|\,\mathcal{E}^{(L)}\,|m^d)(10|\,\mathfrak{M}^{(L')}\,|m^d)^* + (00|\,\mathfrak{M}^{(L)}\,|m^d)(10|\,\mathcal{E}^{(L')}\,|m^d)^*]\},
\end{aligned}
\tag{78}
$$

$$
\begin{aligned}
Q_{23}(\theta) = {} & \tfrac{1}{3}\mathrm{Re} \sum_{L\,L'\,m^d} \{[d^{(L)}_{1\,1-m^d}(\theta)\, d^{(L')}_{1\,1-m^d}(\theta) - d^{(L)}_{1\,m^d-1}(\theta)\, d^{(L')}_{1\,m^d-1}(\theta)] \\
& \times [(11|\,\mathcal{E}^{(L)}\,|m^d)(11|\,\mathcal{E}^{(L')}\,|m^d)^* + (11|\,\mathfrak{M}^{(L)}\,|m^d)(11|\,\mathfrak{M}^{(L')}\,|m^d)^*] \\
& + [d^{(L)}_{1\,1-m^d}(\theta)\, d^{(L')}_{1\,1-m^d}(\theta) + d^{(L)}_{1\,m^d-1}(\theta)\, d^{(L')}_{1\,m^d-1}(\theta)] \\
& \times [(11|\,\mathcal{E}^{(L)}\,|m^d)(11|\,\mathfrak{M}^{(L')}\,|m^d)^* + (11|\,\mathfrak{M}^{(L)}\,|m^d)(11|\,\mathcal{E}^{(L')}\,|m^d)^*] \qquad (79) \\
& + 2[d^{(L)}_{1\,-m^d}(\theta)\, d^{(L')}_{1\,-m^d}(\theta)] \\
& \times [(00|\,\mathcal{E}^{(L)}\,|m^d)(10|\,\mathcal{E}^{(L')}\,|m^d)^* + (00|\,\mathfrak{M}^{(L)}\,|m^d)(10|\,\mathfrak{M}^{(L')}\,|m^d)^* \\
& + (00|\,\mathcal{E}^{(L)}\,|m^d)(10|\,\mathfrak{M}^{(L')}\,|m^d)^* + (00|\,\mathfrak{M}^{(L)}\,|m^d)(10|\,\mathcal{E}^{(L')}\,|m^d)^*]\}.
\end{aligned}
$$

The total cross section is given by

$$
\sigma_t = \frac{16\pi^2}{3} \sum_{L\,\lambda\,j} \frac{1}{2L+1} \{|\,\mathfrak{I}^{(L)}(\lambda j)\,|^2 + |\,\mathfrak{S}^{(L)}(\lambda j)\,|^2\}. \qquad (80)
$$

TABLE I

MATRIX ELEMENTS $\mathfrak{I}^{(L)}(\lambda j)$ AND $\mathfrak{S}^{(L)}(\lambda j)$ FOR THREE ENERGIES IN APPROXIMATION *I*

$Lj\lambda$	$\mathfrak{I}^{(L)}(\lambda j)$ (10^{-3} fermi)			$Lj\lambda$	$\mathfrak{S}^{(L)}(\lambda j)$ (10^{-3} fermi)		
	20 MeV	80 MeV	140 MeV		20 MeV	80 MeV	140 MeV
103	−11.68	−2.477	−1.744	102	6.800	1.770	0.935
112	−.255	−.361	−.378	111	0.283	0.369	0.404
114	39.25	15.46	9.398	113	−.453	−.703	−.679
121	−33.81	−4.345	0.051	122	−3.322	−5.688	−5.580
123	21.40	13.70	11.028	124	−.369	−.572	−.506
211	−.032	.032	.087	212	0.272	0.338	0.341
213	−1.855	−1.273	−1.004	214	0.938	1.153	1.112
222	−.122	−.334	−.383	221	−1.828	−1.673	−.894
224	2.956	1.528	0.868	223	0.545	0.311	0.117
231	−2.705	−2.418	−1.967	232	−.056	−.247	−.352
233	−1.611	−.094	0.484	234	−.333	−1.468	−2.153
321	−.058	−.051	−.052	322	0.111	0.250	0.259
323	−.188	−.235	−.249	324	0.016	0.026	0.023
332	−.002	−.012	−.023	331	−.019	−.049	−.048
334	0.262	0.394	0.428	333	−.017	−.049	−.073
341	−.153	0.002	0.082	342	−.021	−.251	−.507
343	0.207	0.444	0.658	344	−.004	−.037	−.074

For neutron–proton capture, the results are

$$\frac{d\sigma^c}{d\Omega} = I_0^c(\theta)[1 + P_t\, \Sigma^c(\theta) \sin\phi], \tag{81}$$

$$\frac{d\sigma^c}{d\Omega}\, \Sigma_{x'} = I_0^c(\theta)\, \Sigma_{x0}(\theta) + P_t\, Q_{x1}^c(\theta) \sin\phi, \tag{82}$$

$$\frac{d\sigma^c}{d\Omega}\, \Sigma_{y'} = P_t\, Q_{y2}^c(\theta) \cos\phi + P_l\, Q_{y3}^c(\theta), \tag{83}$$

$$\frac{d\sigma^c}{d\Omega}\, \Sigma_{z'} = P_t\, Q_{z2}^c(\theta) \cos\phi + P_l\, Q_{z3}^c(\theta), \tag{84}$$

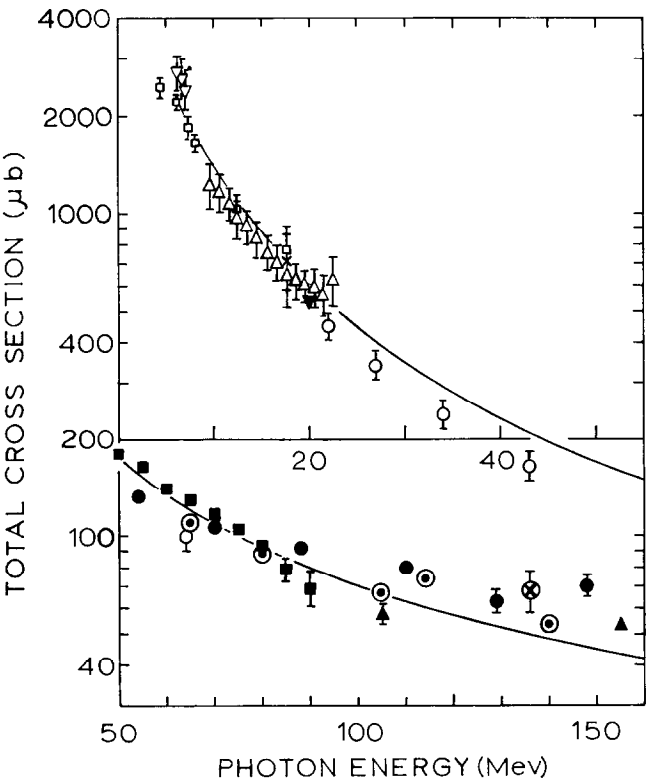

FIG. 3. Total cross section as a function of energy. The solid curve represents our calculation in approximation *I*. The experimental values are shown as follows: hollow circle for Allen, Jr.; solid circle for Alexandrov *et al.*; double circle for Whalin *et al.*; circle with cross for Dixon and Bandtel; hollow square for Barnes *et al.*; solid square for Galey; hollow triangle for Whetstone and Halpern; Hollow inverted triangle for Phillips *et al.*; solid triangle for Keck and Tollestrup; solid inverted triangle for Halpern and Weinstock; cross for Waeffler and Younis and also for Hough.

with $\Sigma_{x'}$, $\Sigma_{y'}$, $\Sigma_{z'}$ defined by Eq. (23), and

$$P_t \equiv [P_x^2(1) + P_y^2(1)]^{1/2} = P_x(1) = \text{transverse polarization of nucleon 1,} \quad (85)$$

$$P_l \equiv P_z = \text{longitudinal polarization of nucleon 1,} \quad (86)$$

$$I_0^c(\theta) = \tfrac{3}{2}(\omega^2/k^2) I_0(\theta), \quad (87)$$

$$\Sigma^c(\theta) = -P_{y0}(\theta), \quad (88)$$

$$\Sigma_{x0}(\theta) = \Sigma(\theta), \quad (89)$$

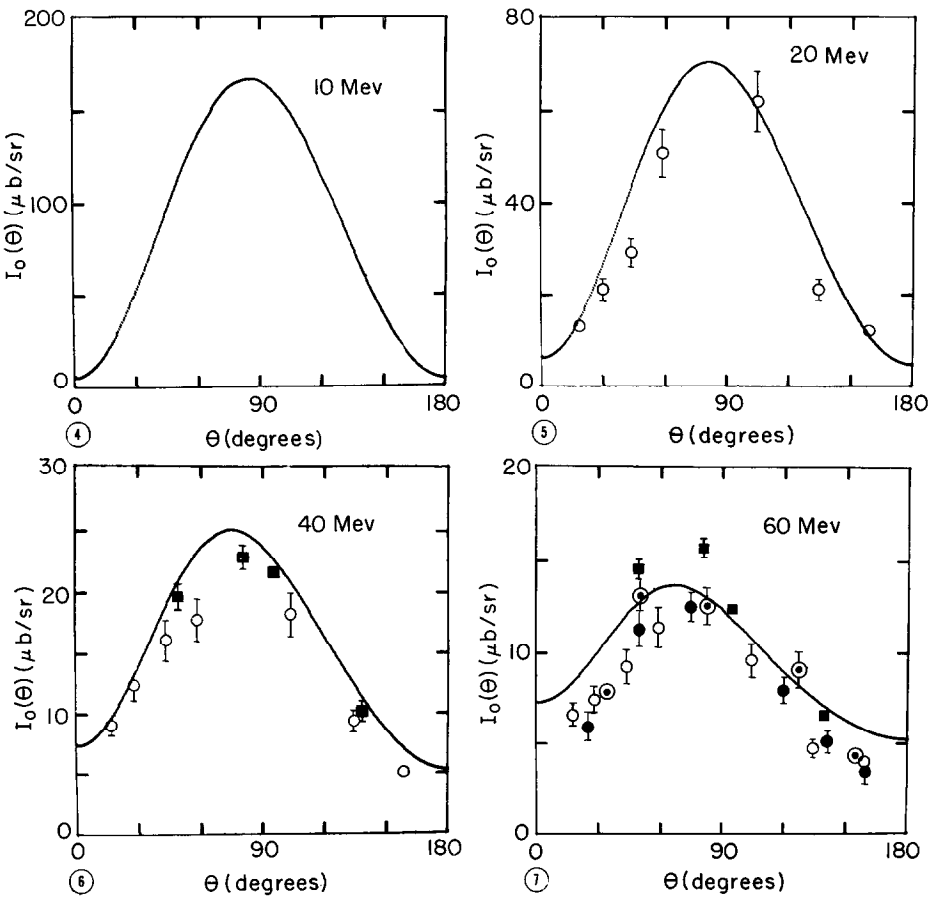

FIGS. 4–7

FIGS. 4–11. Differential cross section in approximation I for photoprotons with initially unpolarized photons of different energies. The experimental values are shown as follows: hollow circle for Allen, Jr.; solid circle for Alexandrov *et al.*; double circle for Whalin *et al.*; solid square for Galey; solid triangle for Keck and Tollestrup.

$$Q^{c}_{x1}(\theta) = -\tfrac{3}{2}(\omega^2/k^2)Q_{y1}(\theta), \tag{90}$$

$$Q^{c}_{y2}(\theta) = -\tfrac{3}{2}(\omega^2/k^2)Q_{x2}(\theta), \tag{91}$$

$$Q^{c}_{y3}(\theta) = \tfrac{3}{2}(\omega^2/k^2)Q_{z2}(\theta), \tag{92}$$

$$Q^{c}_{z2}(\theta) = -\tfrac{3}{2}(\omega^2/k^2)Q_{x3}(\theta), \tag{93}$$

$$Q^{c}_{z3}(\theta) = \tfrac{3}{2}(\omega^2/k^2)Q_{z3}(\theta). \tag{94}$$

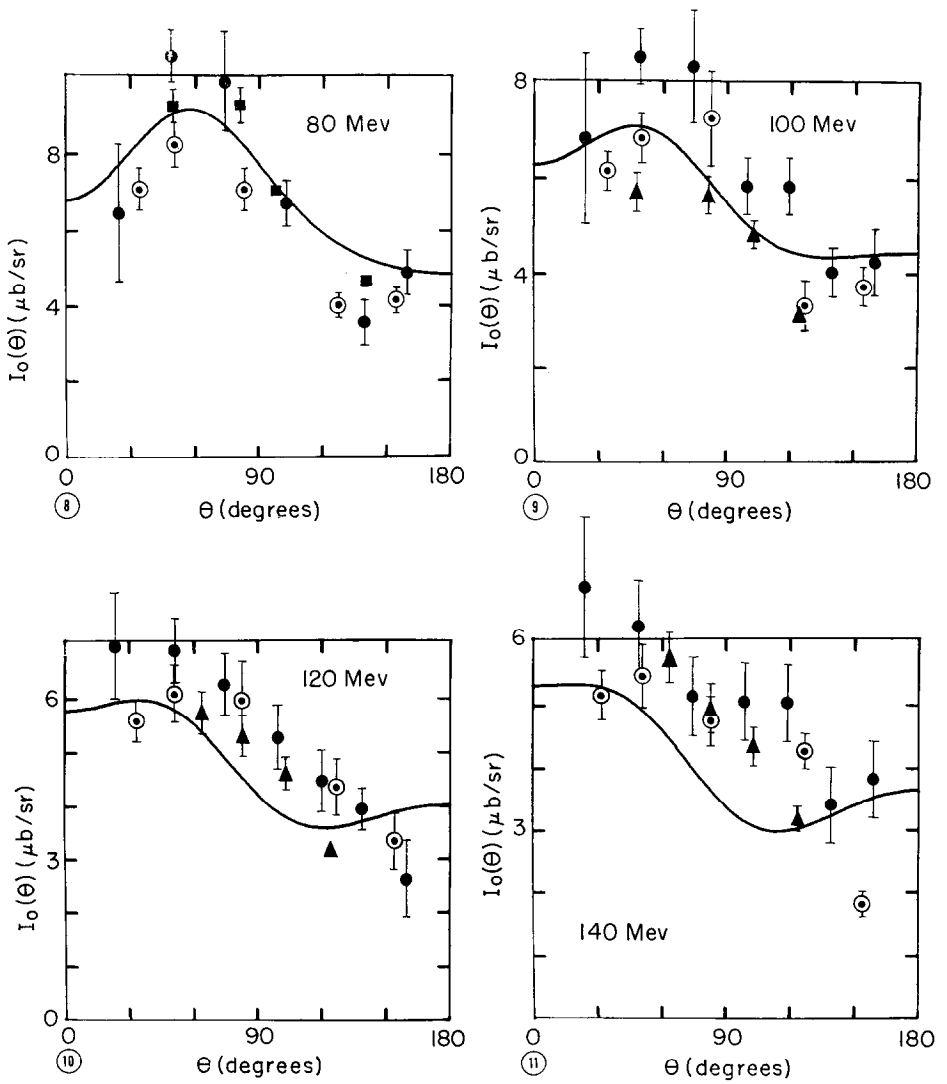

FIGS. 8-11

The total cross section for n–p capture is given by,

$$\sigma_t^c = {}^3\!/_2(\omega^2/k^2)\sigma_t \,. \tag{95}$$

III. RESULTS AND DISCUSSION

Computations were performed on the IBM 7090 Data Processing System at M.I.T. A program for calculating all the cross section and polarization results has been prepared with the following features:

1. The electromagnetic interaction is treated in full with but two approximations: (a) exchange currents and electromagnetic structure of nuclei are neglected. (b) multipole terms higher than dipole-octupole interference have been dropped. All possible transitions within this framework have been taken into account. Provisions have been made to delete or include any particular term (or terms) contributing to the transitions.

2. The wave functions needed for the deuteron and the continuum states are calculated with the same or different internucleon potentials by the Kutta-Gill method. The wave functions can also be computed from a boundary condition model (*21*).

3. The radial integrals (54)–(56) are computed by using the exact wave functions and the exact value of the spherical Bessel functions.

In our computations the internucleon potential of Hamada (*7*) was used for both the deuteron and continuum wave functions. To explore the effect of different terms in the interaction, most computations were performed in ten approximations, as follows.

Approximation A: Only the ordinary $E1$ transitions, induced by the first term (i.e., all the terms within the first summation symbol) of Eq. (52) with $L = 1$, have been included. Retardation is neglected in as much as the contribution

TABLE II

PHOTODISINTEGRATION TOTAL CROSS SECTION σ_t AND COEFFICIENTS, a, b, c, d, e, FOR DIFFERENT ENERGIES IN APPROXIMATION *I*

Energy (MeV)	σ_t (μb)	a (μb/sr)	b (μb/sr)	c (μb/sr)	d (μb/sr)	e (μb/sr)
10	1387.	4.623	162.0	0.3744	29.96	−4.230
20	588.2	5.387	65.50	0.7314	18.25	−4.223
40	224.2	6.236	19.14	0.9983	7.914	−2.164
60	126.6	6.101	7.209	1.001	4.452	−1.564
80	87.40	5.651	3.009	0.9420	2.774	−1.317
100	66.25	5.114	1.025	0.8808	1.812	−.9853
120	53.41	4.618	0.0653	0.8230	1.237	−.7715
140	44.53	4.156	−.4096	0.7737	0.8757	−.6367

coming from the second term of Eq. (38) has been neglected. The spherical Bessel functions, however, have not been replaced by their lowest order expansion.

Approximation B: The singlet $M1$ transitions induced by the fourth term in Eq. (53) with $L = 1$ have been added to approximation A.

Approximation C: The ordinary $E2$ transitions, induced by the first term of Eq. (52) with $L = 2$ have been added to approximation B.

Approximation D: Triplet $M1$ transitions induced by the first term in Eq. (53) with $L = 1$ have been added to approximation C. This term arises from

TABLE III

EFFECT OF DIFFERENT APPROXIMATIONS ON σ_t, a, b, c, d, e, FOR THREE ENERGIES

Energy (MeV)	Approximation	σ_t (μb)	a (μb /sr)	b (μb/sr)	c (μb/sr)	d (μb/sr)	e (μb/sr)
20	A	579.1	4.646	62.16	0.	0.	0.
	B	589.2	5.039	62.77	0.	0.	0.
	C	591.5	5.047	64.12	0.3308	18.32	−1.344
	D	591.7	5.041	64.14	−.1482	18.32	−1.344
	E	591.6	5.070	64.09	0.6955	18.32	−1.344
	F	592.1	5.221	63.88	0.6992	18.31	−1.293
	G	591.9	5.322	63.70	0.6909	18.32	−1.293
	H	588.2	5.356	63.21	0.6939	18.25	−1.293
	I	588.2	5.387	65.50	0.7314	18.25	−4.223
	J	585.1	5.438	65.13	0.7386	18.27	−4.305
80	A	77.15	4.140	2.999	0.	0.	0.
	B	83.50	4.216	3.643	0.	0.	0.
	C	84.55	4.236	4.154	0.4338	2.795	−.5179
	D	84.85	4.222	4.210	−.1799	2.795	−.5179
	E	84.73	4.285	4.100	0.9105	2.795	−.5179
	F	85.43	5.250	2.543	0.9410	2.755	−.2764
	G	90.45	5.648	2.546	0.9284	2.856	−.2764
	H	87.52	5.593	2.279	0.9242	2.759	−.2764
	I	87.40	5.651	3.009	0.9420	2.774	−1.317
	J	86.49	5.871	1.529	1.020	2.157	−.0140
140	A	34.04	2.520	0.2833	0.	0.	0.
	B	39.77	2.655	0.7642	0.	0.	0.
	C	40.38	2.675	1.016	0.3419	0.8738	−.2597
	D	40.67	2.664	1.066	−.0734	0.8738	−.2597
	E	40.55	2.721	0.9667	0.6729	0.8738	−.2597
	F	41.31	3.820	−.7948	0.7449	0.7797	−.0064
	G	47.07	4.191	−.6622	0.7441	0.9243	−.0064
	H	44.64	4.052	−.7445	0.7294	0.8543	−.0064
	I	44.53	4.156	−.4096	0.7737	0.8757	−.6367
	J	42.83	4.149	−1.223	0.8527	0.7727	0.1398

the "orbital" current of the nucleons, and cannot induce transitions to or from an S-state.

Approximation E: Triplet $M1$ transitions induced by spin through the third term of Eq. (53) with $L = 1$ have been added to approximation D.

Approximation F: Triplet $M2$ transitions induced by spin through the third term of Eq. (53) with $L = 2$ have been added to approximation E.

Approximation G: Triplet $E1$ transitions induced by spin through the third term of Eq. (52) with $L = 1$ have been added to approximation F.

Approximation H: The retardation correction to the $E1$ transitions represented

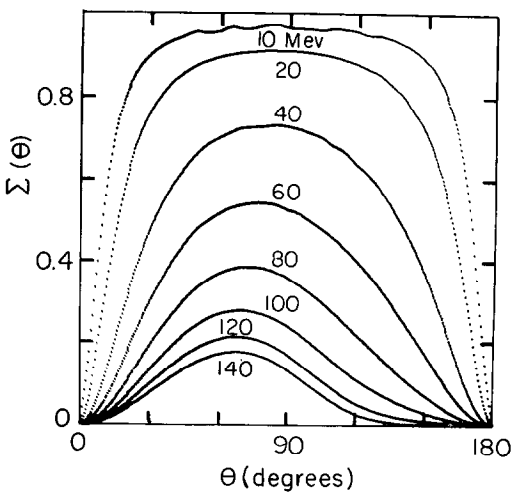

FIG. 12. The function $\Sigma(\theta)$ defined by Eq. (68), as a function of θ for different energies in approximation I (protons are detected).

TABLE IV

COEFFICIENTS f, g, h FOR DIFFERENT ENERGIES COMPUTED IN APPROXIMATION I

Energy (MeV)	f (μb/sr)	g (μb/sr)	h (μb/sr)
10	161.2	29.90	−4.224
20	64.74	18.15	−4.216
40	18.98	7.750	−2.173
60	7.612	4.272	−1.549
80	3.791	2.604	−1.255
100	2.029	1.667	−.8644
120	1.200	1.126	−.5968
140	0.7851	0.8007	−.4100

by the second term of Eq. (52) with $L = 1$ has been added to approximation G. Notice that a part of this correction nearly cancels the relativistic $\omega/2M_d$ correction to the ordinary $E1$ term (first term of Eq. (52)), the part that survives involving only the radial integral I_3.

Approximation I: In this approximation all the terms in Eqs. (52) and (53) have been retained subject to omission of terms of multipolarity higher than dipole-octupole interference. The terms added in this approximation consist of all the terms in approximation H with remaining values of L, the fourth term in

TABLE V

EFFECT OF DIFFERENT APPROXIMATIONS ON f, g, h FOR THREE ENERGIES

Energy (MeV)	Approximation	f (μb/sr)	g (μb/sr)	h (μb/sr)
20	A	62.16	0.	0.
	B	61.55	0.	0.
	C	62.89	18.32	−1.344
	D	62.91	18.32	−1.344
	E	62.89	18.32	−1.344
	F	62.95	18.34	−1.394
	G	62.98	18.34	−1.394
	H	62.49	18.27	−1.394
	I	64.74	18.15	−4.216
	J	64.36	18.17	−4.298
80	A	2.999	0.	0.
	B	2.356	0.	0.
	C	2.881	2.795	−.5179
	D	2.910	2.795	−.5179
	E	2.870	2.795	−.5179
	F	3.470	2.828	−.7595
	G	3.728	2.929	−.7595
	H	3.456	2.832	−.7595
	I	3.791	2.604	−1.255
	J	2.411	1.986	0.0099
140	A	0.2833	0.	0.
	B	−.1977	0.	0.
	C	0.0700	0.8738	−.2597
	D	0.0969	0.8738	−.2597
	E	0.0604	0.8738	−.2597
	F	0.7290	0.9069	−.5130
	G	1.063	1.052	−.5130
	H	0.9428	0.9815	−.5130
	I	0.7851	0.8007	−.4100
	J	−.1598	0.7113	0.4840

Eq. (52) which induces spin EL transitions to singlet states ($L = 1, 2, 3$), the second, fifth, and sixth term of Eq. (53), which induce triplet ML transitions due to orbital current, triplet ML transitions due to spin, and singlet ML transitions due to spin, respectively. These terms involve spherical Bessel func-

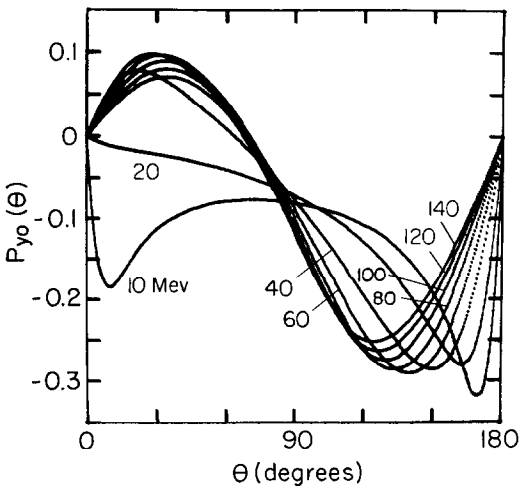

FIG. 13. Polarization of the photoprotons in approximation I for unpolarized incident photons of different energies.

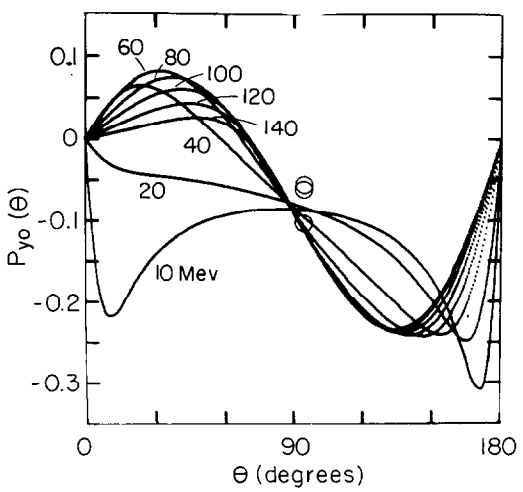

FIG. 14. Polarization of the photoneutrons in approximation I for unpolarized incident photons of different energies. The experimental data, represented by circles, are those of Bertozzi *et al.* The three points correspond, top to bottom, to 13.5, 17.5, and 24 MeV incident photons.

tions of order $L + 1$, which make them much smaller than the first, third, and fourth term of Eq. (53), respectively. They will accordingly be considered with $L = 1, 2$ only.

Approximation J: Same as approximation *I* but with $j_l(z)$ replaced by $z^l/(2l + 1)!!$ in Eqs. (54)–(56).

In photodisintegration the detected nucleon (nucleon 1) can be chosen to be a proton or a neutron. Thus one would get two different sets of cross section and polarization functions. The differential cross section for protons at (θ, ϕ) has the same value as that for neutrons at $(\pi - \theta, \pi + \phi)$. No such relation exists for polarization parameters.

In n–p capture the proton is usually the target. Therefore, the neutron is considered nucleon No. 1.

Exposition of Results

Results are contained in Tables I–VII and in Figs. 3 through 28. The following conventions are used in the graphs.

a. All angles are center of mass (CM) angles.

b. All energies are laboratory energies. In the case of photodisintegration, the energy is the laboratory energy of the photon, while in the case of n–p capture, it is the laboratory energy of the neutron.

TABLE VI

Coefficients i, j, k, l for Different Energies Computed in Approximation *I* for Protons and Neutrons

Detected nucleon	Energy (MeV)	i (μb/sr)	j (μb/sr)	k (μb/sr)	l (μb/sr)
Proton	10	−13.29	1.678	−.0872	−.0237
	20	−4.517	3.994	−.3834	−.0881
	40	−1.291	3.917	−.5204	−.1339
	60	−.5862	2.980	−.4775	−.1795
	80	−.3512	2.274	−.3974	−.2270
	100	−.2610	1.735	−.3061	−.2386
	120	−.2247	1.361	−.2300	−.2477
	140	−.2122	1.095	−.1646	−.2493
Neutron	10	−14.56	4.155	0.4507	−.0241
	20	−6.184	5.176	0.8162	−.0847
	40	−2.929	4.335	0.9585	−.1167
	60	−2.057	3.227	0.9841	−.1487
	80	−1.660	2.470	0.9735	−.1891
	100	−1.419	1.913	0.9417	−.1988
	120	−1.263	1.530	0.9075	−.2092
	140	−1.155	1.255	0.8736	−.2118

Photodisintegration Results

Matrix Elements

Table I gives the matrix elements $\mathfrak{I}$ and $\mathfrak{S}$ defined by Eqs. (52) and (53) for three energies in approximation I. Each matrix element gives the transition amplitude of multipolarity L from the deuteron state to an eigenstate (λj) of the continuum. $\mathfrak{I}$ corresponds to electric and $\mathfrak{S}$ to magnetic transitions.

TABLE VII

Effect of Different Approximations on i, j, k, l for Protons for Three Energies

Energy (MeV)	Approximation	i (μb/sr)	j (μb/sr)	k (μb/sr)	l (μb/sr)
20	*A*	0.	4.428	0.	0.
	B	−5.222	4.428	.	0.
	C	−4.620	3.899	−.6196	.00177
	D	−4.972	3.923	−.6196	.00177
	E	−4.366	3.876	−.6196	.00177
	F	−4.359	3.991	−.5227	.00717
	G	−4.442	3.947	−.5050	.00717
	H	−4.431	3.931	−.5030	.00717
	I	−4.517	3.994	−.3834	−.0881
	J	−4.470	3.991	−.3841	−.0900
80	*A*	0.	2.185	0.	0.
	B	−.8405	2.185	0.	0.
	C	−.1904	2.152	−.6979	−.0264
	D	−.2129	2.184	−.6979	−.0264
	E	−.1773	2.113	−.6979	−.0264
	F	−.2244	2.224	−.6026	−.0061
	G	−.2342	2.266	−.5929	−.0061
	H	−.2339	2.154	−.5660	−.0061
	I	−.3512	2.274	−.3974	−.2270
	J	−.3746	2.083	−.3470	−.0979
140	*A*	0.	0.9943	0.	0.
	B	−.4736	0.9943	0.	0.
	C	−.0505	0.9647	−.4909	−.0493
	D	−.0766	0.9966	−.4909	−.0493
	E	−.0314	0.9230	−.4909	−.0493
	F	−.0768	1.037	−.3633	−.0364
	G	−.0783	1.090	−.3761	−.0364
	H	−.0838	0.9654	−.3367	−.0364
	I	−.2122	1.095	−.1646	−.2493
	J	−.2122	0.7142	−.0552	−.0699

Total Cross Section

Figure 3 shows a plot of the total cross section against energy calculated in approximation *I*, together with experimental points (*22*). The agreement is good. The calculated values are also to be found in Table II. In Table III the effect of ten different approximations on the total cross section is included for three energies. It is evident that dipole transitions account for the main part of the total cross section at all energies considered, but whereas at 20 MeV electric dipole plays a dominant role in the total cross section, at higher energies other dipole effects become increasingly important. Magnetic dipole spin flip has an

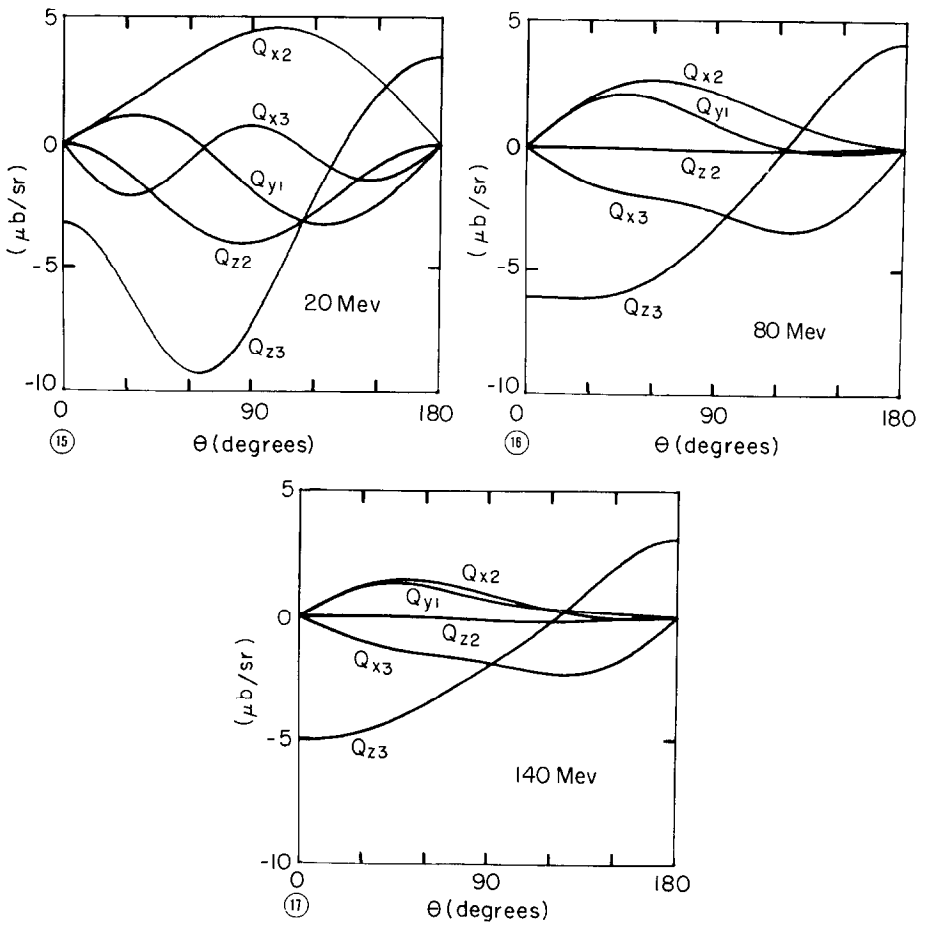

FIGS. 15–17. Polarization functions $Q_{x2}(\theta)$, $Q_{x3}(\theta)$, $Q_{y1}(\theta)$, $Q_{z2}(\theta)$, $Q_{z3}(\theta)$, for photoprotons at different energies.

8% effect at 80 MeV and a 16% effect at 140 MeV. Triplet $E1$ transitions induced by spin, not considered previously, increase the total cross section by 6% at 80 MeV and by 14% at 140 MeV. Finally the retardation correction to $E1$ transitions, included in approximation H, produces a 3% decrease at 80 MeV and a 5% decrease at 140 MeV.

Differential Cross Section

Let us consider first the differential cross section with unpolarized incident photons, $I_0(\theta)$. When the vast discrepancy among different experimental data

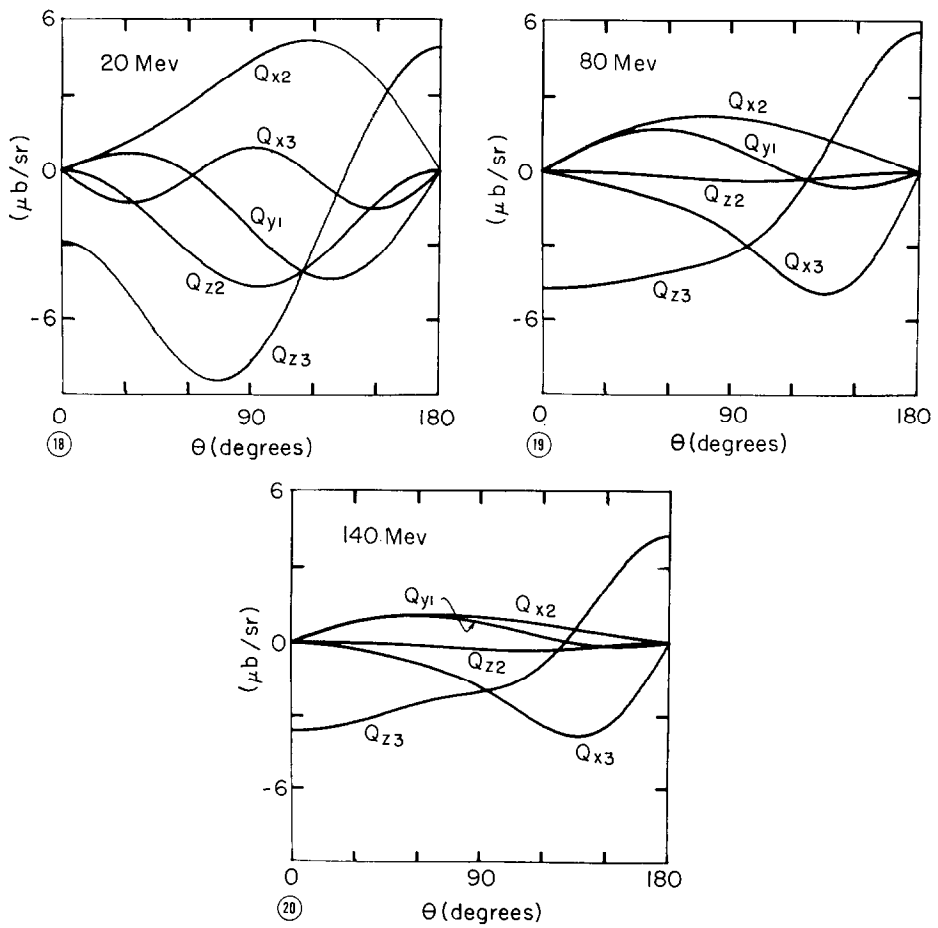

FIGS. 18-20. Polarization functions $Q_{x2}(\theta)$, $Q_{x3}(\theta)$, $Q_{y1}(\theta)$, $Q_{z2}(\theta)$, $Q_{z3}(\theta)$, for photoneutrons at different energies.

is taken into account, the result for $I_0(\theta)$ seems to fit them reasonably well except for 120 and 140 MeV. Figures 4 through 11 show the calculated cross section for different photon energies in approximation I together with experimental points. In this approximation we may write

$$I_0(\theta) = a + b \sin^2 \theta + c \cos \theta + d \sin^2 (\theta) \cos \theta + e \sin^4 (\theta). \quad (96)$$

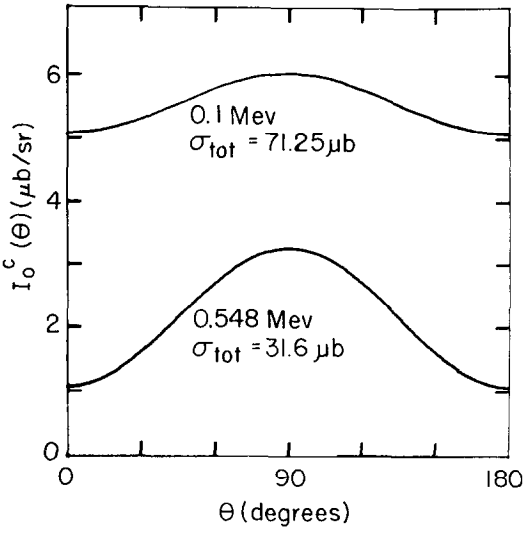

FIG. 21. Neutron–proton capture differential and total cross section at two different neutron energies.

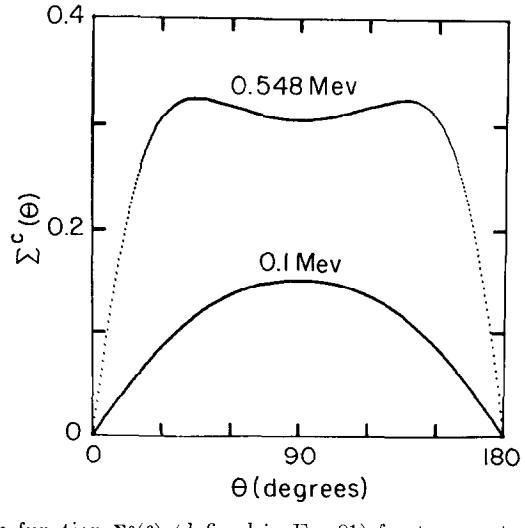

FIG. 22. The function $\Sigma^c(\theta)$ (defined in Eq. 81) for two neutron energies

Table II lists the calculated values of the coefficients a, b, c, d, e for various energies in approximation I. Table III compares the same coefficients calculated in all ten approximations at three energies. Note the dramatic effect at higher energies of triplet $M2$ term due to spin, introduced in approximation F. Approxi-

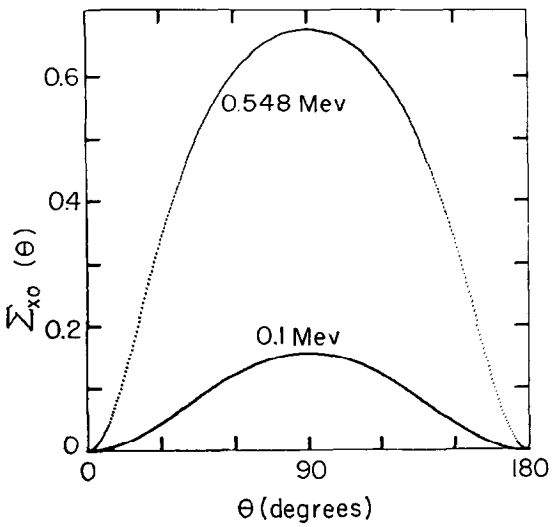

FIG. 23. The photon polarization parameter $\Sigma_{x0}(\theta)$ for unpolarized incident neutrons (see Eq. (82)) at two energies.

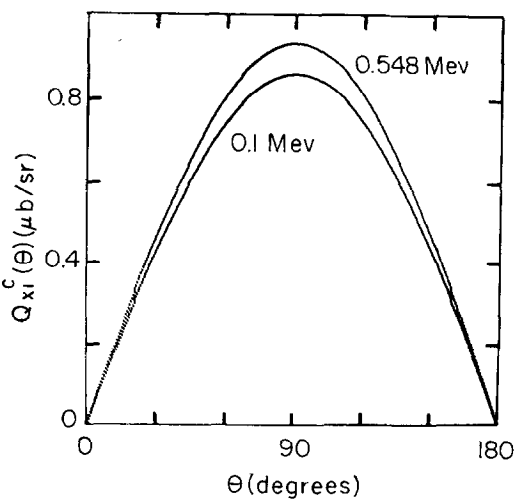

FIG. 24

FIGS. 24–28. Other photon polarization functions, $Q^c_{x1}(\theta)$, $Q^c_{y2}(\theta)$, $Q^c_{y3}(\theta)$, $Q^c_{z2}(\theta)$, and $Q^c_{z3}(\theta)$ (see Eqs. (82)-(84)) for two neutron energies.

mation I, which incorporates all the terms in dipole and quadrupole transitions not included in H plus all the octupole effects, differs only slightly from approximation H, indicating the relatively minor role of those terms.

For polarized incident photons, the additional function $\Sigma(\theta)$ is needed (see Eq. (68)). Figure 12 contains plots of $\Sigma(\theta)$ calculated in approximation I for different energies. In this approximation we may write

$$I_0(\theta)\Sigma(\theta) = f \sin^2(\theta) + g \sin^2(\theta) \cos\theta + h \sin^4(\theta). \tag{97}$$

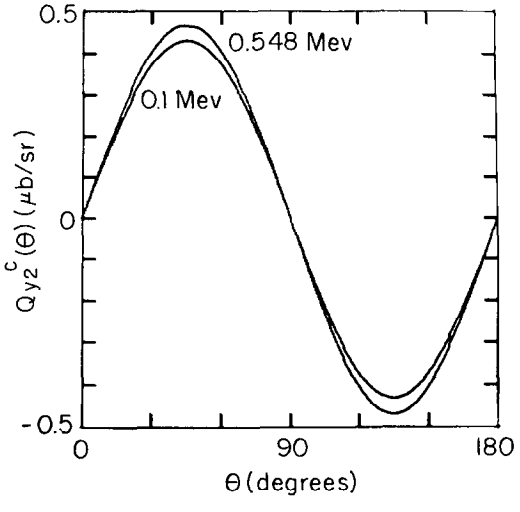

FIG. 25

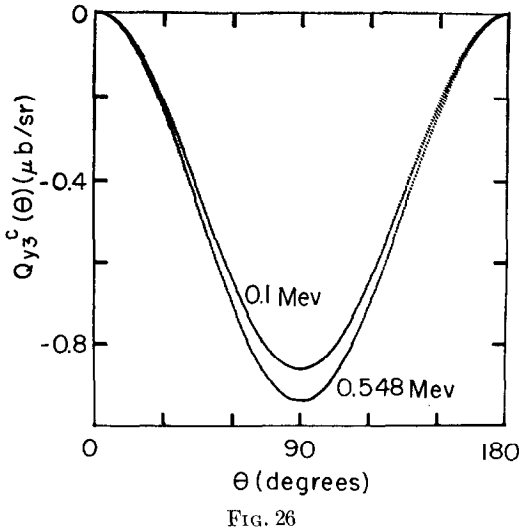

FIG. 26

Table IV lists the calculated values of the coefficients f, g, h for different energies in approximation I. Table V compares the same coefficients calculated in different approximations at three energies. Note the large effect of triplet $M2$ transitions included in approximation F, especially at higher energies.

Polarization

The nucleon polarization for unpolarized incident photons is in the y-direction (i.e. in the $\boldsymbol{\omega} \times \mathbf{k}$ direction) owing to parity conservation, and is given by $P_{y0}(\theta)$

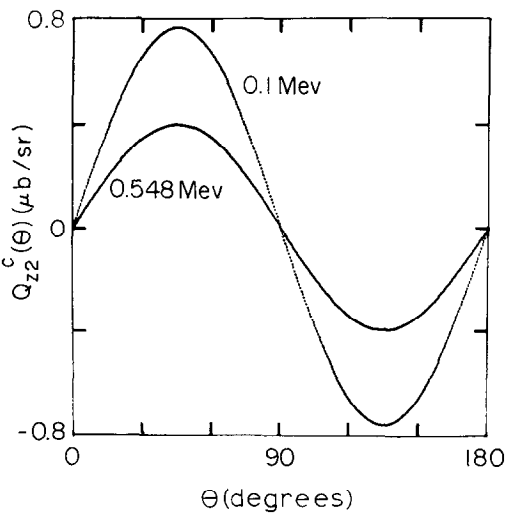

FIG. 27

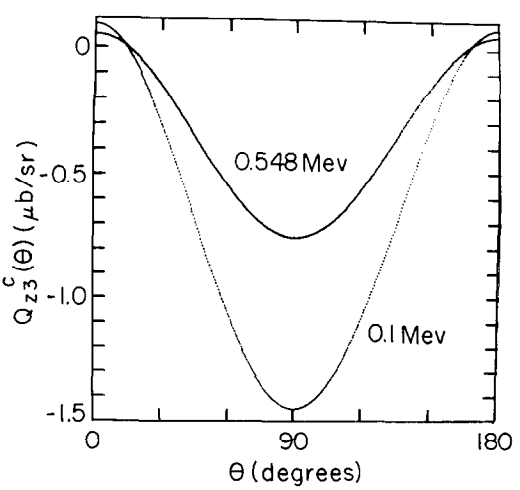

FIG. 28

(see Eq. (70)). This function is plotted in Fig. 13 for protons and in Fig. 14 for neutrons at different energies, all in approximation *I*. Figure 14 includes some experimental points obtained by Bertozzi *et al.* (*22*). Table VI lists the value of the coefficients i, j, k, l in the expansion,

$$I_0(\theta)P_{y0}(\theta) = i \sin\theta + j \sin\theta \cos\theta + k \sin^3\theta + l \sin^3\theta \cos\theta, \qquad (98)$$

for protons and neutrons at different energies in approximation *I*. Table VII compares the same coefficients for protons in different approximations for three energies. Since $M1$ spin flip interferes with $E1$ in the expression for $P_{y0}(\theta)$, its role is greatly enhanced, as seen in Table VII.

For initially polarized photons, five other functions are needed to completely describe the final polarization. These are $Q_{x2}(\theta)$, $Q_{x3}(\theta)$, $Q_{y1}(\theta)$, $Q_{z2}(\theta)$, and $Q_{z3}(\theta)$, as defined by Eqs. (69), (70), and (71). Figures 15, 16, and 17 show these parameters for protons at 20, 80, and 140 MeV, respectively, while Figs. 18, 19, and 20 give the same functions for neutrons.

Neutron–Proton Capture Results

Our result for thermal capture cross section is much too low because of the small singlet scattering length predicted by Hamada's potential. However, our calculations show that the cross section is larger by 2% when computed from exact wave functions than from approximate zero-range wave functions using the singlet scattering length predicted by Hamada's potential. It is thus conceivable that, using exact wave functions from a potential that fits the singlet scattering length better than Hamada's, one may be able to eliminate the 5% discrepancy now existing between the experimental cross section and that calculated from zero-range theory.

Figures 21–28 show capture cross section and polarization parameters for the two neutron energies 0.1 and 0.548 MeV. In the limit of zero energy, the only functions not vanishing are $I_0^c(\theta)$, $Q_{z2}^c(\theta)$, and $Q_{z3}^c(\theta)$, the last two giving the circular polarization of the photon due to the transverse and longitudinal neutron polarization, respectively. The circular polarization, however, does not exceed 3% at 0.025 eV.

CONCLUSIONS

We conclude that the generally ignored spin $E1$ transitions and spin $E2$ transitions to triplet states are important, producing measurable changes at photon energies higher than 80 MeV. Octupole transitions produce an appreciable change only at the highest energies considered, but higher multipoles are not needed. The electromagnetic structure of the nucleons may well not be significant as their dimensions are small compared to the nuclear separation. It would, however, be an easy matter to incorporate the experimentally known nuclear form factors in this calculation, modifying Eqs. (46) and (47). This would isolate the

relativistic and exchange effects, which must then account for any discrepancy with experiment (assuming a satisfactory internucleon potential).

With Hamada's potential a 2% improvement is gained in the thermal n–p capture cross section by using exact wave functions. It is possible that other potentials that fit the singlet scattering length better than Hamada's may afford an even closer approach to the experimental zero-energy capture cross section.

ACKNOWLEDGMENTS

The author is indebted to Professor Herman Feshbach for suggesting this problem, his inspiring supervision of it, and for reviewing the manuscript; to Professor Earle L. Lomon for valuable discussions and for reviewing the manuscript; to the M.I.T. Joint Computation Center for the time made available on the I.B.M. 7090; and to Dr. C. Shakin for providing the subroutines for computing Clebsch-Gordan and related coefficients.

RECEIVED: September 9, 1963

REFERENCES

1. J. J. DESWART AND R. E. MARSHAK, *Physica* **25,** 1001 (1959).
2. M. L. RUSTGI, W. ZERNIK, G. BREIT, AND D. J. ANDREWS, *Phys. Rev.* **120,** 1881 (1960).
3. W. ZICKENDRAHT, D. J. ANDREWS, M. L. RUSTGI, W. ZERNIK, A. J. TORRUELLA, AND G. BREIT, *Phys. Rev.* **124,** 1538 (1961).
4. G. KRAMER AND C. WERNTZ, *Phys. Rev.* **119,** 1627 (1960).
5. A. DONNACHIE, *Nucl. Phys.* **32,** 637 (1962).
6. F. PARTOVI, *Ann. Phys. (N. Y.)* **27,** 114–132 (1964).
7. T. HAMADA AND I. D. JOHNSTON, *Nucl. Phys.* **34,** 382 (1962).
8. J. J. DESWART, *Physica* **25,** 233 (1959).
9. U. FANO, *Rev. Mod. Phys.* **29,** 74 (1957). (Note the slightly different definition.)
10. M. E. ROSE, "Elementary Theory of Angular Momentum," 2nd printing, Chap. IV, p. 52. Wiley, New York, 1961.
11. L. D. PEARLSTEIN AND A. KLEIN, *Phys. Rev.* **118,** 193 (1960).
12. SHIH-HUI HSIEH, *Progr. Theoret. Phys.* **21,** 585 (1959).
13. T. AKIBA, *Progr. Theoret. Phys.* **24,** 370 (1960).
14. R. HOFSTADTER, F. BUMILLER, AND M. CROISSIAUX, *Phys. Rev. Letters* **5,** 261, 263 (1960).
15. R. HOFSTADTER AND C. DEVRIES, *Phys. Rev. Letters* **6,** 290 (1961).
16. R. HOFSTADTER AND R. HERMAN, *Phys. Rev. Letters* **6,** 298 (1961).
17. D. N. OLSON, H. F. SCHOPPER, AND R. R. WILSON, *Phys. Rev. Letters* **6,** 286 (1961).
18. R. M. LITTAUER, H. F. SCHOPPER, AND R. R. WILSON, *Phys. Rev. Letters* **7,** 141, 144 (1961).
19. G. RACAH, *Phys. Rev.* **62,** 438 (1942).
20. M. ROTENBERG, R. BIVINS, N. METROPOLIS, AND J. K. WOOTEN, JR., "The 3-*j* and 6-*j* Symbols," pp. 1, 13, 19. The Technology Press, Massachusetts Institute of Technology, Cambridge, Massachusetts, 1959.
21. H. FESHBACH, E. LOMON, AND L. TUBIS, *Phys. Rev. Letters* **6,** 635 (1961). The neutron–proton fits are also available now and will be published.
22. The experimental data given in the following papers have been used: IU.A. ALEXANDROV, N. B. DELONE, L. I. SOLOVOKHOTOV, G. A. SOKOL, AND L. N. SHTARKOV, *Zh. Eksperim. i Teor. Fiz.* **33,** 614(1957), transl. *Soviet Phys.-JETP* **6,** 472 (1958); L. ALLEN, JR., *Phys. Rev.* **98,** 705 (1955); C. A. BARNES, J. H. CARVER, G. H. STAFFORD, AND

D. H. Wilkinson, *Phys. Rev.* **86,** 359 (1952); D. R. Dixon and K. C. Bandtel, *Phys. Rev.* **104,** 1730 (1956); J. A. Galey, *Phys. Rev.* **117,** 763 (1960); J. Halpern and E. V. Weinstock, *Phys. Rev.* **91,** 934 (1953); P. V. C. Hough, *Phys. Rev.* **80,** 1069 (1950); J. C. Keck and A. V. Tollestrup, *Phys. Rev.* **101,** 360 (1956); J. A. Phillips, J. S. Lawson, and P. G. Kruger, *Phys. Rev.* **80,** 326 (1950); H. Waeffler and S. Younis, *Helv. Phys. Acta* **24,** 483 (1951); B. A. Whalin, B. D. Schriever, and A. O. Hanson, *Phys. Rev.* **101,** 377 (1956); A. L. Whetstone and J. Halpern, *Phys. Rev.* **109,** 2072 (1958); W. Bertozzi, P. Demos, S. Kowalski, C. P. Sargent, W. Turchinetz, R. Fullbood, and J. Russell, *Phys. Rev. Letters* **10,** 106 (1963).